AFCRL-67-0107

# FERROMAGNETIC DOMAIN STUDIES IN HIGHLY PERFECT METAL PLATELETS AND WHISKERS

R. W. DeBlois

General Electric Research and Development Center

Contract No. AF19(628)-5804

Project No. 4600

Task No. 460003

FINAL REPORT

Period Covered: 1 December 1965 to 30 November 1966

March 1967



Prepared for

AIR FORCE CAMBRIDGE RESEARCH LABORATORIES
OFFICE OF AEROSPACE RESEARCH
UNITED STATES AIR FORCE
BEDFORD, MASSACHUSETTS 01730

## ABSTRACT

Nearly perfect thin single-crystal platelets and submicron whiskers of nickel and nickel alloy are used to study nearly ideal ferromagnetic domain and domain wall structures and behavior. Applying fields to classically simple domain patterns leads to new observations of surface pinning and to the formation of several new types of double walls. One type is composed of 180° walls of mixed Néel-Bloch structure. Domain observations at the edges and corners of Ni-Co and Ni-Fe platelets with weak negative anisotropy reveal a new "tulip" pattern that makes clear the process of formation of edge echelons and corner chevrons. Precise determinations of saturation fields at platelet corners and ends are made by examining the resulting domain pattern at low field. Nucleation at the corners and edges of previously saturated thin platelets is observable in low positive and negative fields. Further platelet observations include a field induced stripe pattern in Ni-Co platelets with positive anisotropy, domain walls formed by magnetostrictive anisotropy, and details of spin directions in 180° domain walls with various sequences of Bloch walls, Néel walls, and Bloch lines.

Individual single-domain nickel whiskers as thin as 600 Å have been optically observed, handled, and tested in ferromagnetic nucleation studies. Physical buckling of the whiskers into forms of the elastica permits one to measure both end and infinite-cylinder nucleation fields. Observed fields vs whisker diameter and vs field angle follow curling theory. Thickness comparisons by electron microscopy and by bending yield an effective Young's modulus near $10 \times 10^{11}$ dyn/cm$^2$, about half the handbook value.

TABLE OF CONTENTS

# FERROMAGNETIC DOMAIN STUDIES IN HIGHLY PERFECT METAL PLATELETS AND WHISKERS

R. W. DeBlois

## I. INTRODUCTION

The ferromagnetic domain and domain wall properties of nearly perfect single-crystal platelets and whiskers of nickel and nickel alloy have been the subject of this investigation. The platelets range in thickness from less than 1000 Å to over $10^5$ Å and are thus of thin-film thickness. Their perfection in terms of internal crystal structure, surface smoothness, and edge sharpness, and their simple geometric forms make them ideal specimens for extending prior thin-film domain studies. In general, whatever structures can be seen in thin films can now be seen more clearly and in more nearly perfect form in the platelets, since the imperfections that are always found in thin films are absent. The simplicity of the observed structures in the platelets may lead to greater understanding of the structure and behavior of thin films. It should also lead to more precise checks on ferromagnetic domain theory since discrepancies between theory and experiment must now generally reflect on the adequacy of the theory.

The following study illustrates many features of ferromagnetic domain and domain wall structure and behavior. New observations of this study include:[1-3] (1) a domain wall intermediate in structure between the classical Bloch and Néel walls; (2) a double wall formed of two intermediate walls; (3) edge closure domains that form a "tulip" pattern and that reveal how the more commonly observed echelon pattern forms; (4) an interaction between a 180° Bloch wall and a platelet edge that may lead to new knowledge on surface pinning; (5) saturation and nucleation at platelet corners and in submicron nickel whiskers; and (6) a field induced stripe pattern.

Platelets and whiskers of nickel and nickel-cobalt are readily grown in large quantities by the hydrogen reduction of the metal halides.[1, 2] The Ni-Co alloy has been especially useful for this study because it has positive magnetocrystalline anisotropy in the range of 4% to 18% cobalt. Thus, its domain structures are different from and generally simpler than those of nickel. Nickel-iron platelets of the Permalloy composition, 81% nickel, have just recently been successfully grown for the first time. This is of significance because it is the zero-magnetostriction composition that is used for thin-film memory elements.

Some general references (page 62) on ferromagnetism and ferromagnetic domains are listed after the specific references in this report. These may prove useful for providing background material that it would be impractical to include here.

BLANK PAGE

## II. FERROMAGNETIC DOMAIN STRUCTURE AND BEHAVIOR

### A. Introduction

Weiss first postulated the existence of ferromagnetic domains in 1907 in order to explain how a piece of iron can apparently be unmagnetized at room temperature while, according to the Curie-Weiss law that he developed, iron as a material should have a high intensity of magnetization even in zero field.[4] With domains, different parts of the iron can be fully magnetized, but in various directions, so that the total magnetization of the specimens adds up vectorially to zero. But it was not till the 1930's, with the theories of Bloch[5] and of Landau and Lifshitz[6] concerning the structures of domain walls and closure domains, that domain studies began to develop into one of the major realms of ferromagnetism. Since the behavior of ferromagnetic materials from transformer steels to thin-film memory elements depends to a large extent on domain structure and behavior, the current technological importance of such studies is evident.

The near perfection of the nickel and Ni-Co platelets makes them ideal specimens for various ferromagnetic domain studies. The imperfections in most crystals restrain the motion of domain walls, thus giving rise to nonequilibrium configurations with hysteresis, remanence, and coercivity. But the domain structures observed in the platelets are in stable or metastable equilibrium, and the domain walls move reversibly, without hysteresis, as long as the topological structure is not broken. In addition, the low indices of the surfaces and edges of the platelets lead to structures that are often classically simple, and are thus highly suitable both for theoretical analysis and for illustrating various phenomena for educational purposes.

### B. Simple Domain Structures

Figure 1(a) is a photomicrograph (Bitter technique) illustrating the simplest possible closure domain in a Ni-Co platelet 165 μm wide and with positive magnetocrystalline anisotropy. Figure 1(b) illustrates an alternative simple closure structure. [R. Gemperle has recently observed similar patterns in iron platelets.[7]] For both patterns the magnetocrystalline anisotropy and the magnetostatic energies are a minimum since in each domain the magnetization lies along an easy ⟨100⟩ direction and since there are no edge or surface poles formed except at the domain walls, where the magnetic moments, or spins, rotate over a distance of about 1000 Å from one direction to another. The second structure contains more domain wall energy than the first, but one further energy term to account for is that from magnetostriction since each domain tends to contract along the direction of magnetization. This strain energy is less for the subdivided second structure than for the first.[8] Thus it is not immediately clear which structure has the lower total energy. As will be shown, either structure can be formed at will by following prescribed magnetization procedures.

In small applied fields the domain walls move reversibly ($H_c < 0.01$ Oe). Figure 1(c) shows the equilibrium form that developed from Fig. 1(a) when a

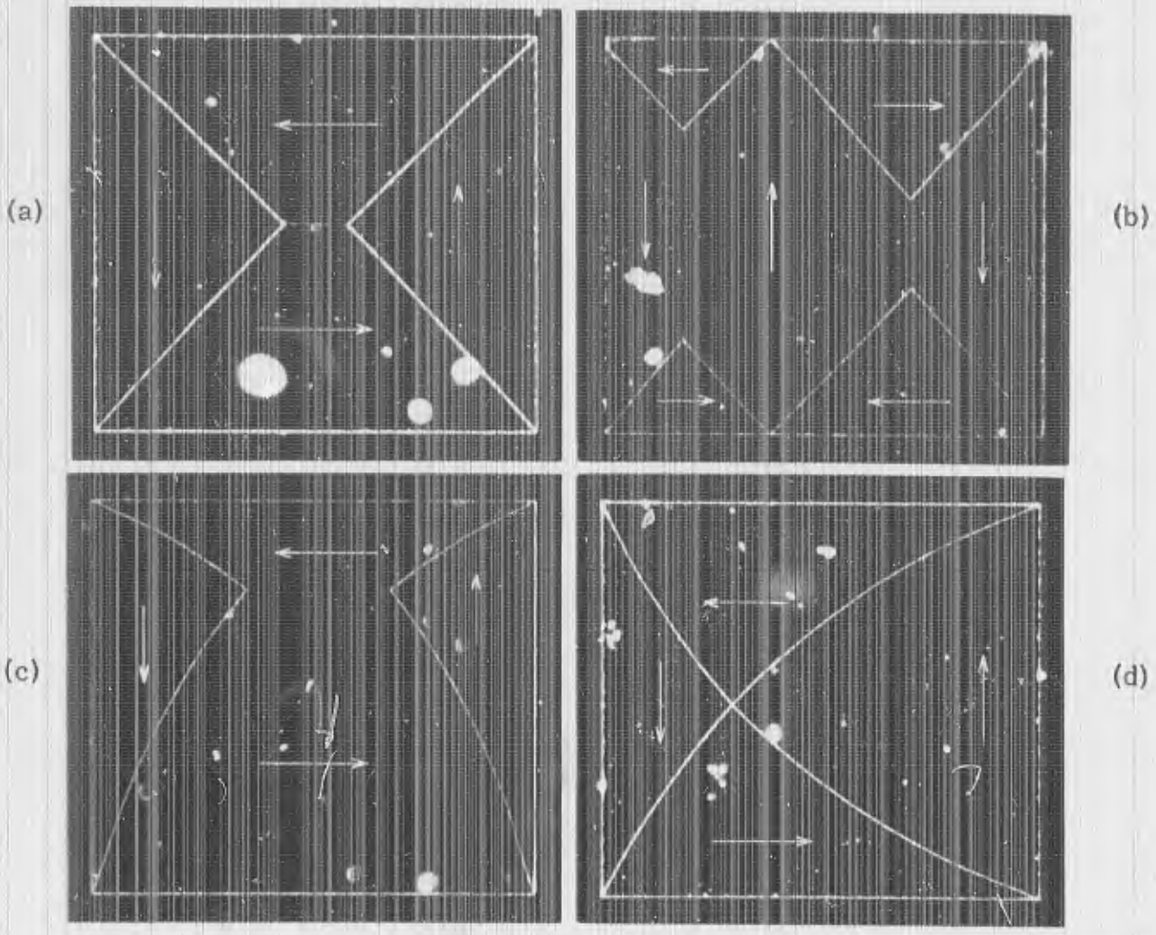


Fig. 1 Simple ferromagnetic domain patterns in a single-crystal Ni-Co platelet: (a) and (b) are two alternative zero-field closure patterns; (c) shows the changed pattern of (a) in a field of 3.6 Oe to the right; and (d) shows the changed pattern of (a) in an upward field of 3.9 Oe.

field of 3.6 Oe was applied to the right, and Fig. 1(d) shows the form in a vertical field of 3.9 Oe. In both cases the domain with its magnetization pointing in the field direction grows in area. Two features of significance are that the domain walls stick to the corners and that the domain walls curve to form arcs of circles. The corner behavior is related to the problem of the motion of domain walls past inclusions; the curvatures yield a measure of the net fields acting along the domain walls. If the normal component of magnetization across a domain wall is constant, then the net field acting along the wall is

$$H = \gamma_{90}/rM_S \quad \text{or} \quad H = \gamma/2rM_S, \tag{1a, b}$$

for 90° or 180° domain walls, respectively. Here, $\gamma_{90}$ is the energy density of a 90° domain wall, $\gamma$ is that of a 180° wall, r is the radius of curvature, and $M_S$ is the saturation magnetization per unit volume.

The curvature of both the 90° and 180° walls of Fig. 1(c) is 275 μm. If we neglect the free poles that form in the curved walls because the normal components of magnetization are not constant across them, and also assume that the net field acting along the walls of a given domain is constant, then Eqs. (1a) and (1b) show the 180° domain wall energy to be twice that of the 90° domain wall. If $\gamma_{90}$ is assumed to be 0.2 erg $cm^{-2}$ and $M_S$ is taken as 600 emu, then the net field H is 0.012 Oe. These oversimplified calculations lead to an inconsistency in the net field difference between the top and bottom domains of Fig. 1(c), depending upon whether one traces a path across the 180° wall or two 90° walls. But they do indicate how effectively the readjustment in the domain structure and the formation of free poles within the walls and at the edges shield the interior of the crystal from the applied field,[2, 7] and they also reveal the existence of a neat problem in magnetostatics.

In a field of 4.1 Oe applied to the right the structure of Fig. 1(c) snapped irreversibly to that shown in Fig. 2. This change in structure does involve a loss of energy. Thus the platelets will display hysteresis if the applied fields are large enough to change the domain pattern topology.

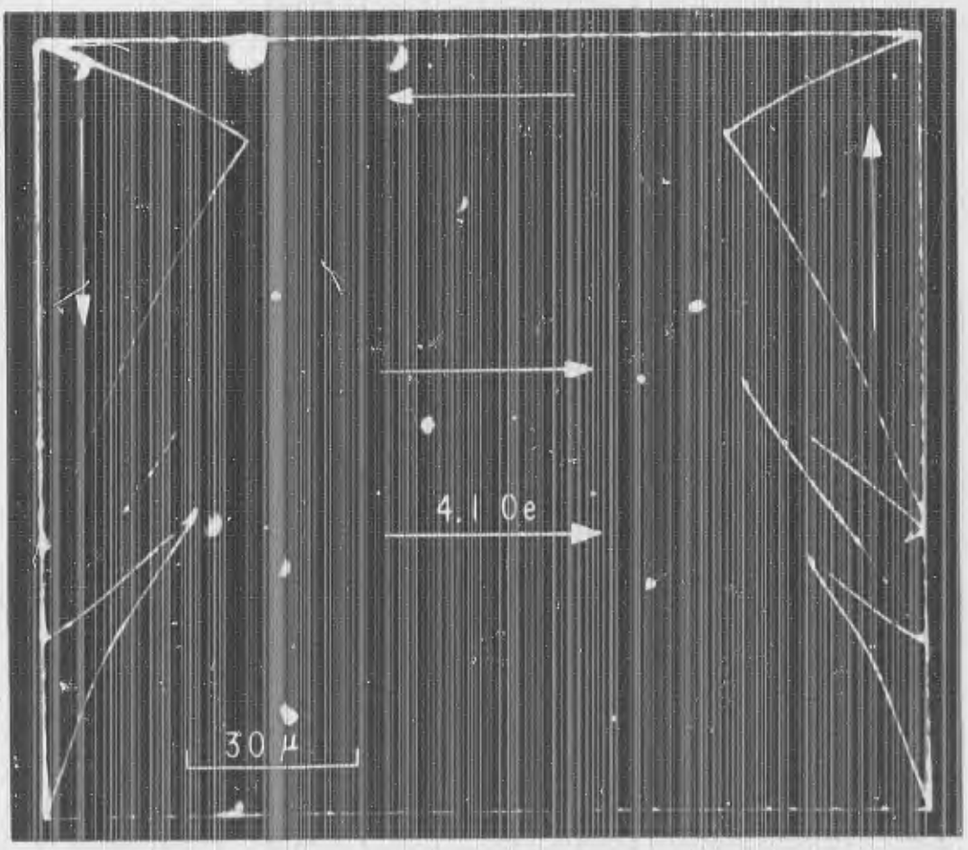


Fig. 2 Irreversible change in pattern (c) of Fig. 1 in a field of 4.1 Oe to the right.

C. Surface Pinning

In a higher field of 5.2 Oe the central 180° domain wall of Fig. 2 moved to the edge of the platelet (Fig. 3) but did not part, even though the projections of the arcs extend beyond the edge of the platelet. When the field was reduced, the wall moved away from the edge to again form the structure of Fig. 2. That a Bloch wall can press against the edge of a platelet and still not unwind and part is surprising. It indicates that the magnetic spins at the edge are rotationally restrained. This might arise from surface anisotropy or, more generally, surface pinning,[9-15] and further studies of this phenomenon, which has been observed in many platelets, should increase our knowledge of this surface effect.

Figure 4(a) shows another example of surface pinning, this time at a ⟨110⟩ edge of a nickel right triangular platelet in a planar field of 13.3 Oe applied perpendicular to the edge. Figure 4(b), taken later at a reduced field of 5 Oe, shows that the central 180° domain wall was still continuous when part of it was pressing against the edge. More detailed observations of this structure revealed that the 180° domain wall snapped to the edge when it approached to within about 1 μm. Thus, the edge effect does not merely oppose the rotation of the spins, but also makes the edge an energetically favorable position for the wall. A field reduction of about 0.6 Oe was needed to snap the wall away from the edge. (Of this, about 0.1 Oe appeared to be due to a wall motion coercive force; this was determined by repositioning the wall after moving it toward the edge, but not bringing it close enough to snap on. Surface corrosion by the Bitter solution is generally observed to produce a detectable coercive force after many minutes of immersion.)

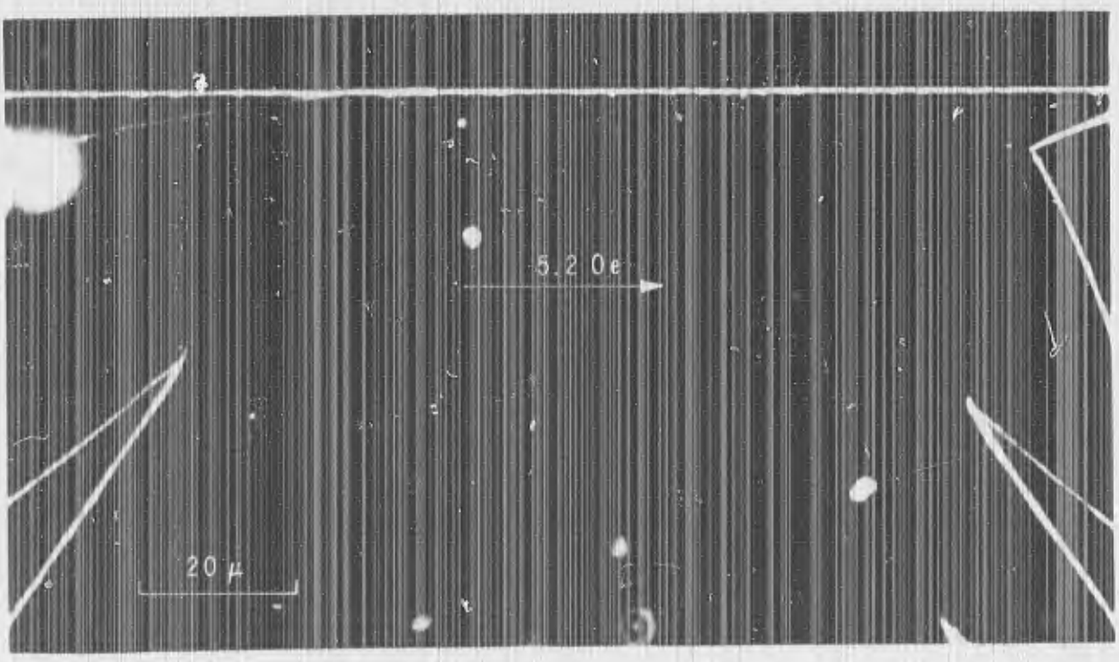


Fig. 3 Upper central region of the same platelet and pattern of Fig. 2 in an increased field of 5.2 Oe to the right, showing the 180° Bloch wall pressing against the platelet edge without parting.

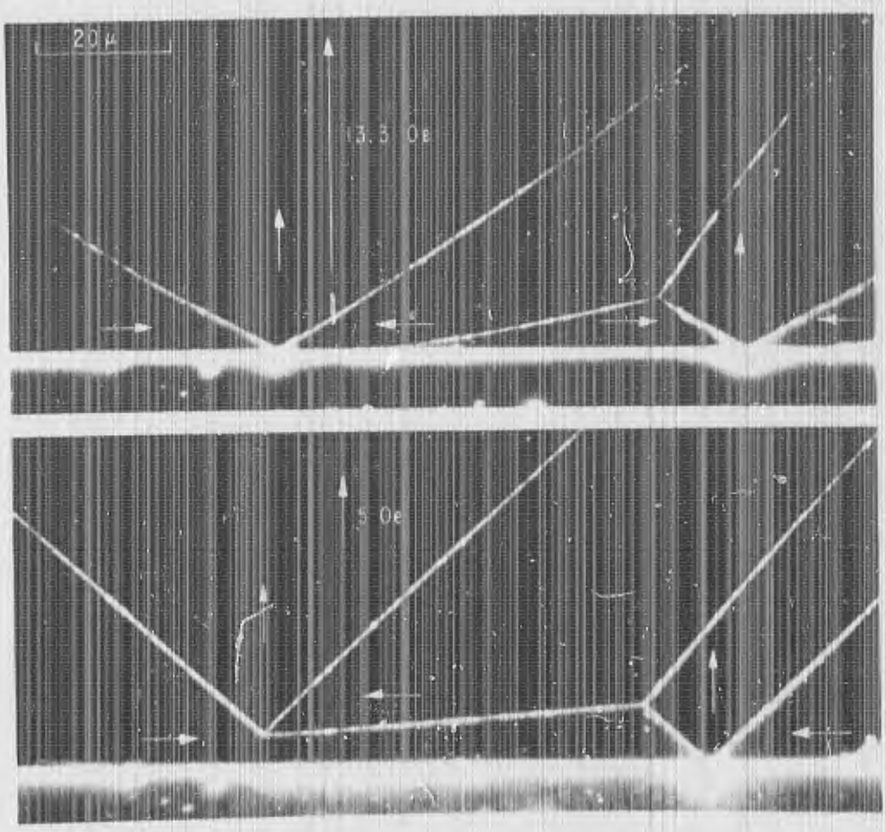


Fig. 4(a) Domain walls at the edge of a nickel platelet in a 13.3 Oe field. The lower central domain wall is pinned at the platelet edge. (b) Domain walls in a reduced field of 5 Oe, showing that the lower central domain wall was continuous in Fig. 4(a).

D. Diagonal Field Structures

Figure 5(a) shows a Ni-Co platelet in a field of 6.5 Oe applied diagonally toward the upper right. The magnetization zigzags along this general direction from one wedge-shaped domain to the next, but points in an easy direction, parallel to an edge, in each. The structure thus avoids large demagnetizing fields by maintaining the magnetization at the base of each wedge approximately parallel to the edge. The walls themselves are not at 45° with the platelet edges and thus contain some volume free-poles. Figure 5(b) shows the domain structure in an increased field of 35 Oe. The spacing between wedges along the diagonal has remained almost constant. A simple calculation shows that even if we neglect the demagnetizing fields, the 35 Oe field would rotate the magnetization only about 6.5° from the easy directions toward the field direction.

Similar wedge-shaped domains have been studied in thin films, but for films the domain spacing depends largely on local variations of the anisotropy.[16] For platelets, this is an equilibrium structure that should be tractable to analysis

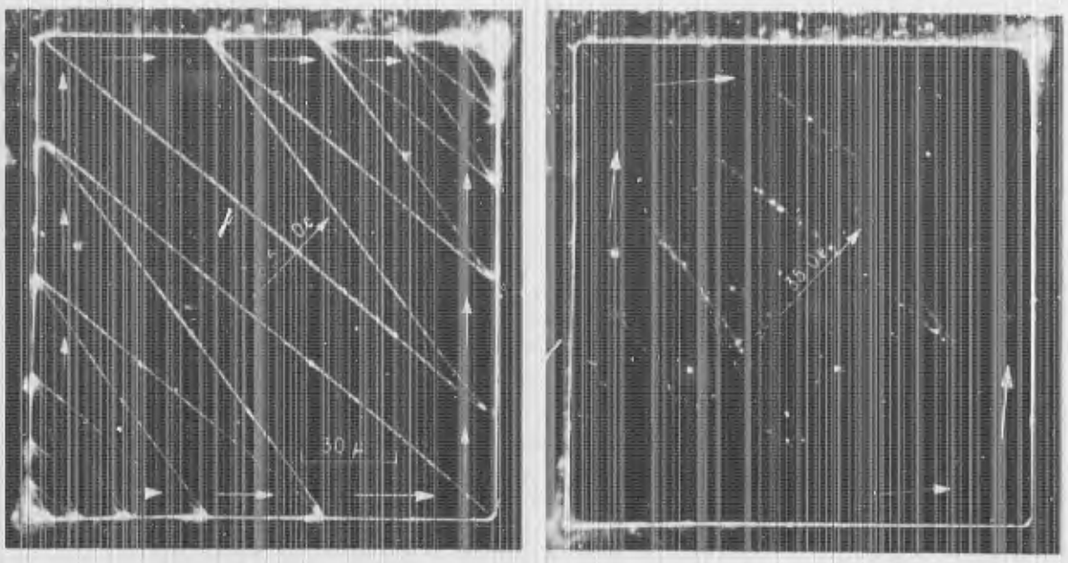


(a) (b)

Fig. 5 (a) Domain pattern in a Ni-Co platelet in a diagonal field of 6.5 Oe. (b) Domain pattern in the same platelet in an increased diagonal field of 35 Oe.

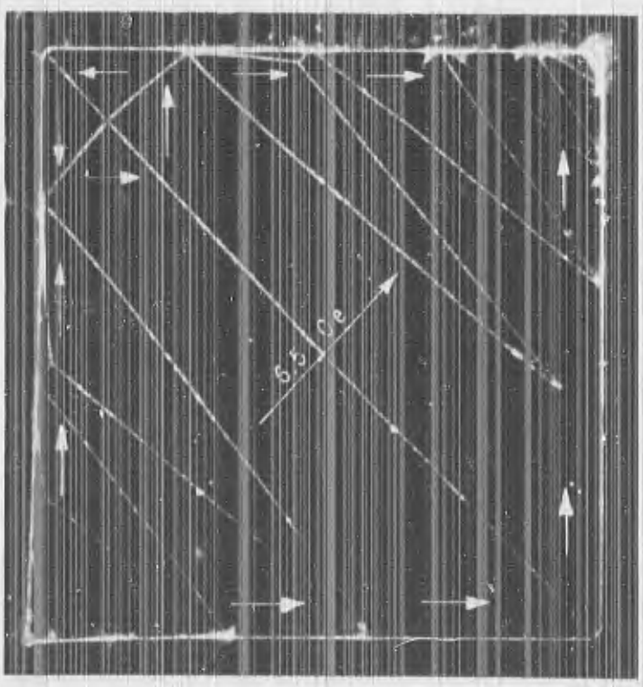


Fig. 6 A variant domain pattern in the Ni-Co platelet of Fig. 5 in a diagonal field of 6.5 Oe.

in terms of anisotropy, domain wall energy, saturation magnetization, and platelet thickness.

Figure 6 shows an easily obtainable variant of Fig. 5(a). The same platelet is again in a diagonal field of 6.5 Oe, but now there is a domain wall extending from corner to corner and a flux closure pattern at the upper-left corner. If the diagonal field is reduced, this closure pattern expands to form the zero-field pattern of Fig. 1(a). On the other hand, if the diagonal field of Fig. 5(a) is reduced, the zero-field pattern becomes that of Fig. 1(b) (with arrows oppositely directed). In this case the magnetization vectors at the corners opposite the field diagonal both zigzag toward the same upper-right corner of Fig. 5(a), and this feature is maintained to zero field. These variant structures emphasize the importance of the applied field history in determining a stable or metastable domain pattern (and as a corollary, the importance of the thermal history as well).

E. Edge and Corner Domains

The closure domain structures shown in Fig. 1 are remarkably simple because the platelet grew with ⟨100⟩ edges and {100} surfaces, and the easy directions of magnetization for the Ni-Co alloy of this platelet lie in the plane, parallel to the edges. In nickel platelets and Ni-Co platelets with negative magnetocrystalline anisotropy ($-K_1$) the easy directions are ⟨111⟩. If the platelet is thin enough ($d \lesssim 0.7\ \mu m$), demagnetizing fields keep the magnetization

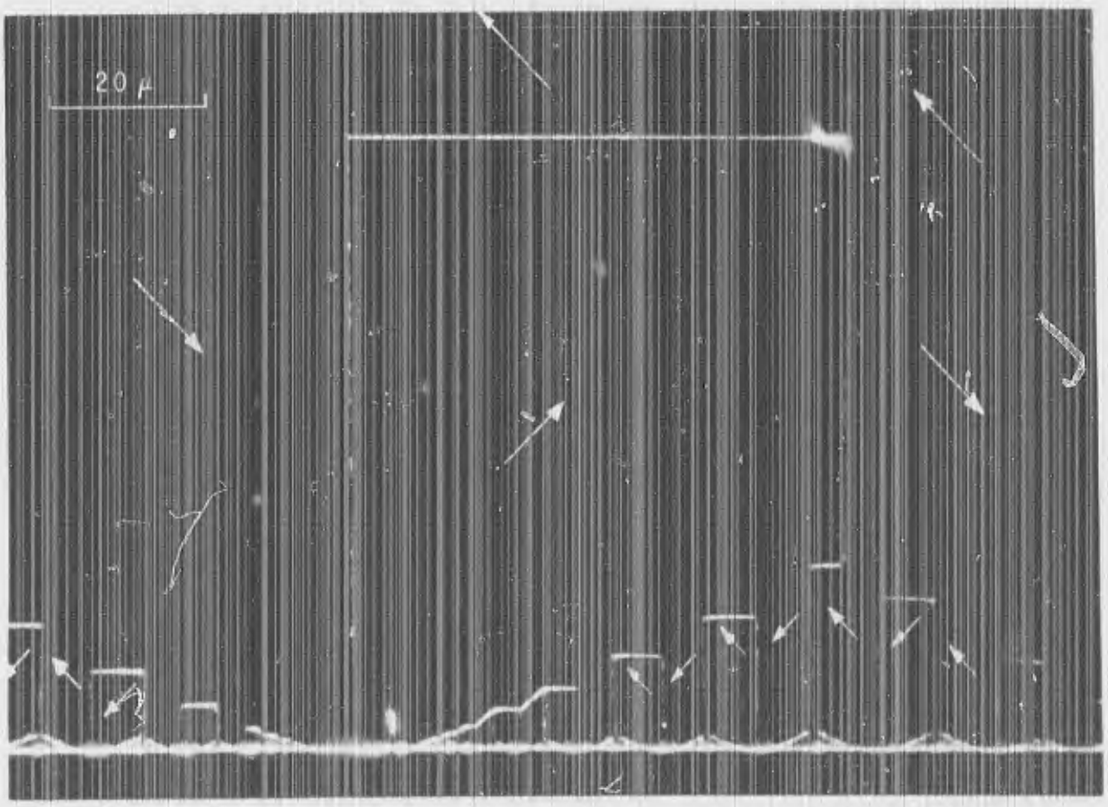


Fig. 7 Echelon pattern at a ⟨100⟩ edge of a nickel platelet 2700 Å thick.

in the plane, so that effectively the easy directions are ⟨110⟩; but still these directions are at 45° with the ⟨100⟩ edges. Therefore, the domain pattern is typically complex and is built up of echelons[17] such as are shown in Fig. 7. (See also Figs. 1-6, and 12 of Ref. 1 and Figs. 5, 6, and 9 of Ref. 2.)

The echelon forms a closure structure that is closely related to the pattern formed in the extensively studied Neel strip,[18-21] and long, narrow nickel ribbons, such as that of Fig. 5, Ref. 1, might advantageously be used to extend these studies (which relate the magnetization curve to the detailed domain structure). These ribbons do, for example, show remanence and also discontinuous reversals of magnetization at approximately $\pm 1$ Oe, both being due to structural details rather than to domain wall coercive force.

At a corner, the echelon structures commonly merge to form the "chevrons" or miter-joint-like structures shown in the nickel platelet of Fig. 8. (Also see Figs. 1 through 3 of Ref. 1 and Fig. 9 of Ref. 2.) For both figures there is a diagonally applied field of 10 Oe, in the first case toward the upper left, and in the second case toward the lower right. The corner structures shown here were formed as diagonally applied fields of several hundred oersteds were applied and reduced to 10 Oe. (These applied fields are incidental to the present discussion, but will become relevant when saturation and nucleation are

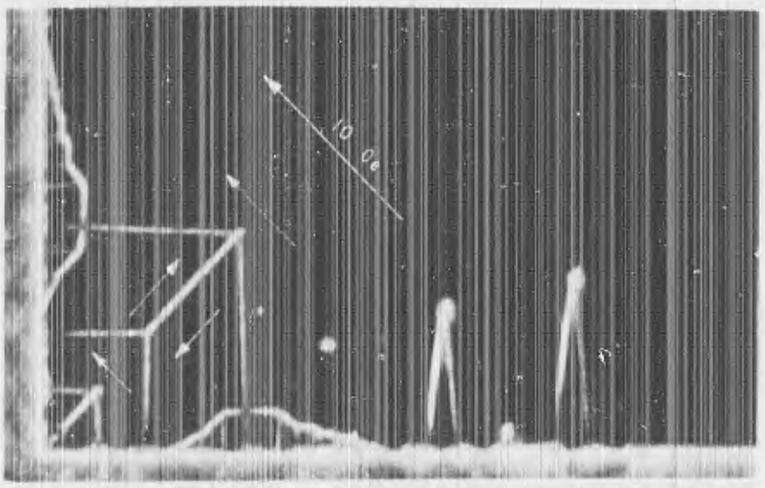


Fig. 8(a) "Chevron" pattern at a corner of a nickel platelet in a diagonal field of 10 Oe to the upper left.

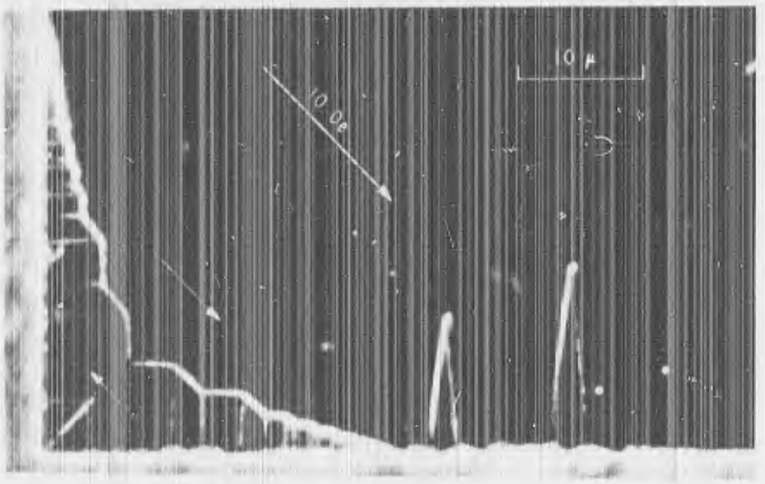


Fig. 8(b) Chevron and echelon pattern at the same corner in a 10 Oe field to the lower right. The magnetization in the corner structure still zigzags toward the upper left.

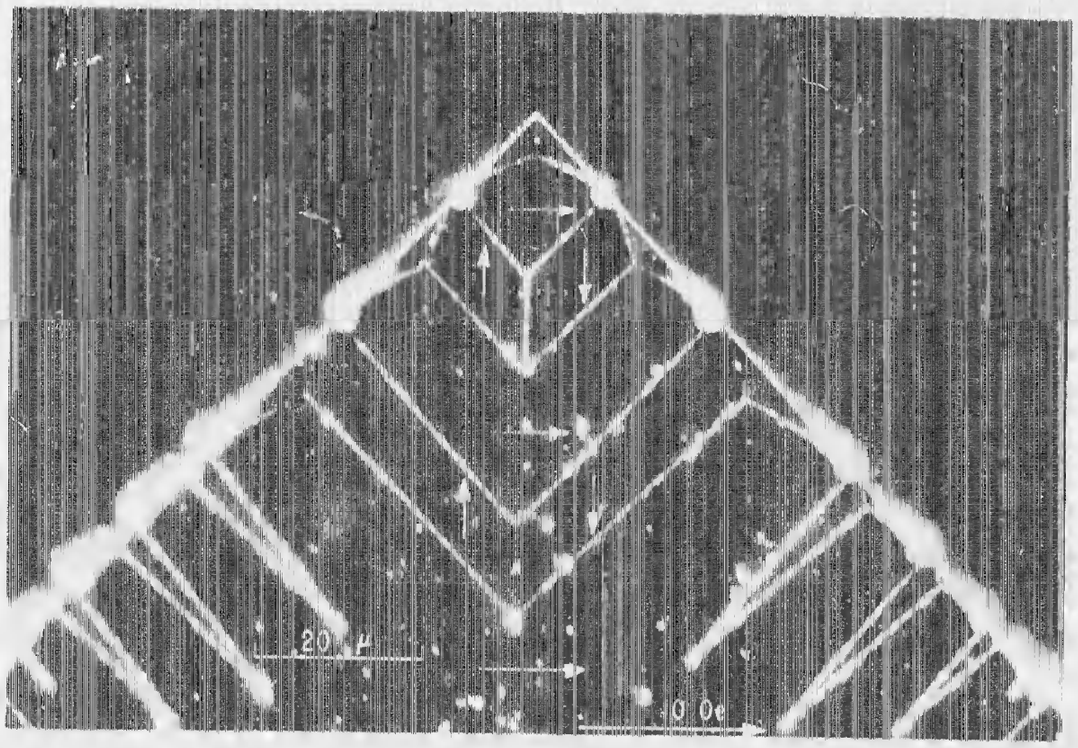


Fig. 9 An alternative corner structure in a nickel platelet in a field of 10 Oe to the right. The magnetization in the two domains at the very corner zigzags toward the left, opposite the field.

discussed.) An alternative corner structure with two triangular domains of reverse magnetization at the very corner is shown in Fig. 9 of another nickel platelet, also in a diagonally applied field of 10 Oe.

Details of edge and corner closure domain structure and formation show up with greater clarity in Ni-Co and Ni-Fe alloys with low magnitudes of $K_1$ than in nickel. The reduced magnetocrystalline anisotropy serves, in effect, to magnify the domain structures. Figure 10(a) shows the domain structure in a Ni-Co platelet with variable composition. To the left it is cobalt-poor and has positive anisotropy; the magnetization is parallel or perpendicular to the ⟨100⟩ edges. To the right the anisotropy is negative and the easy planar directions are ⟨110⟩. (Ni-Co alloys have positive magnetocrystalline anisotropy from about 4% to 18% cobalt.) Figure 10(b) is an enlargement of the region where the anisotropy constant $K_1$ passes through zero. A typical "tulip" pattern forms at the edge in the region of weak negative anisotropy. The transition along the edge from plus to minus anisotropy is quite smooth since even in the negative region there is a triangular region where the magnetization is parallel to the edge.

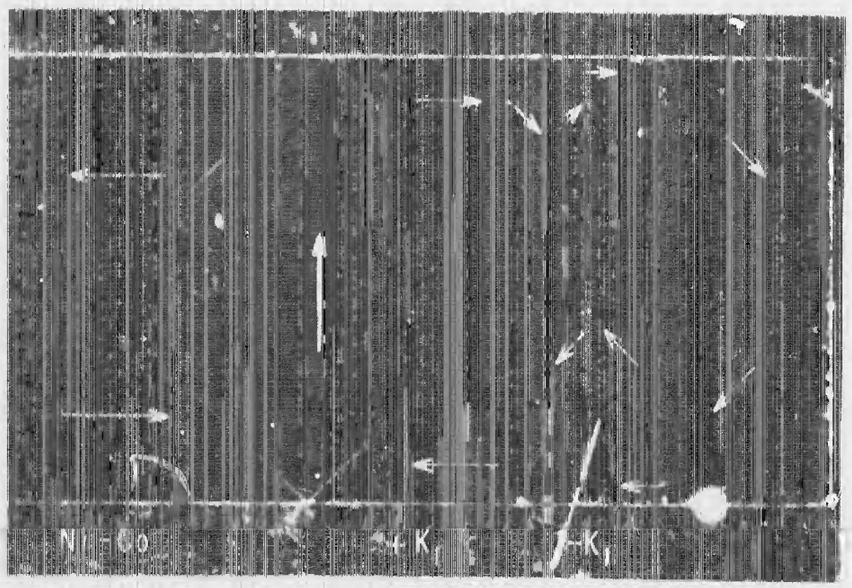


Fig. 10(a) Domain structure in a Ni-Co platelet with variable composition and with positive anisotropy to the left and negative anisotropy to the right.

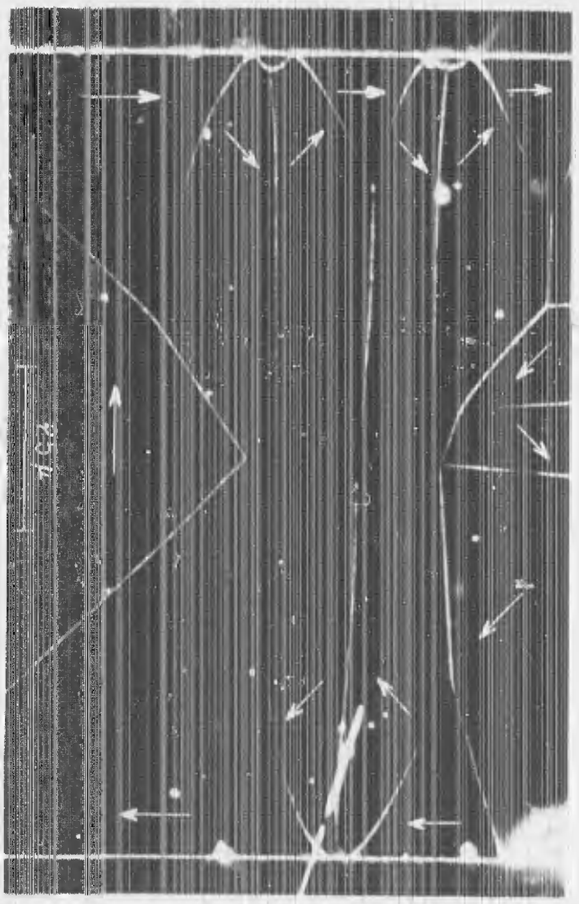

Fig. 10(b) Enlargement of the region where the anisotropy passes through zero. A characteristic "tulip" pattern forms at the edges where the anisotropy is weakly negative.

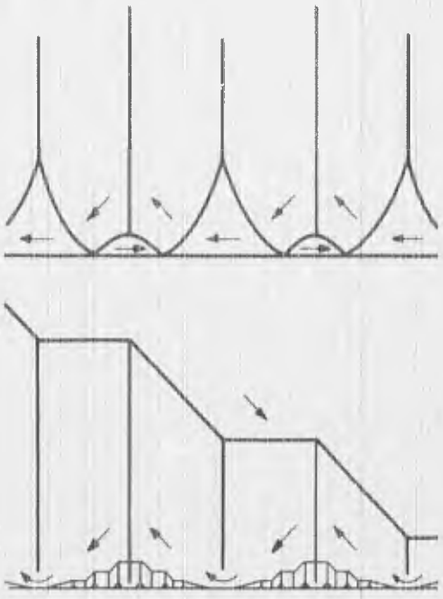

Fig. 11 (a) Schematic "tulip" pattern at a ⟨100⟩ edge of a thin platelet with weak negative anisotropy (or at a ⟨110⟩ edge of a thin platelet with weak positive anisotropy). (b) Echelon pattern into which the above "tulip" pattern develops with stronger negative anisotropy.

Schematic Fig. 11(a) shows the directions of magnetization for the weak-anisotropy "tulip" pattern. The formation of the edge segments magnetized to the right involves nucleation. They need not exist in the less fully developed pattern. The relation between the tulip and echelon patterns becomes evident by comparison of Figs. 11(a) and (b). The edge segments develop into subechelons, which may even further subdivide, and the triangular areas magnetized to the left shrink to form regions of high divergence where the magnetization curves around the tips of the 90° walls.

In a similar manner the corner domain structure of Fig. 12(a) of a Ni-Fe platelet (81% Ni) with low negative anisotropy and zero magnetostriction shows the mode of formation of the chevrons of Fig. 8. With the help of the sketch of Fig. 12(b) it appears that the same tulip pattern of Fig. 11(a) generates the set of chevrons from the corner as the field is reduced or, in a virgin platelet (Fig. 1 of Ref. 1), as the anisotropy increases in magnitude during cooling. As the pattern propagates away from the corner, the diagonal domain wall is pinched off, the triangular domains between "tulips" shrink and form 90° walls, and new tulip patterns form near the corner.

Figure 13 contains a further illustration of the formation of chevrons at the corner and also of the development of the echelon structure. It is to be compared with Fig. 8(b). The sketch is of a corner of the same Ni-Fe platelet of Fig. 12 after a magnetic field had been applied and removed to change the virgin domain structure.

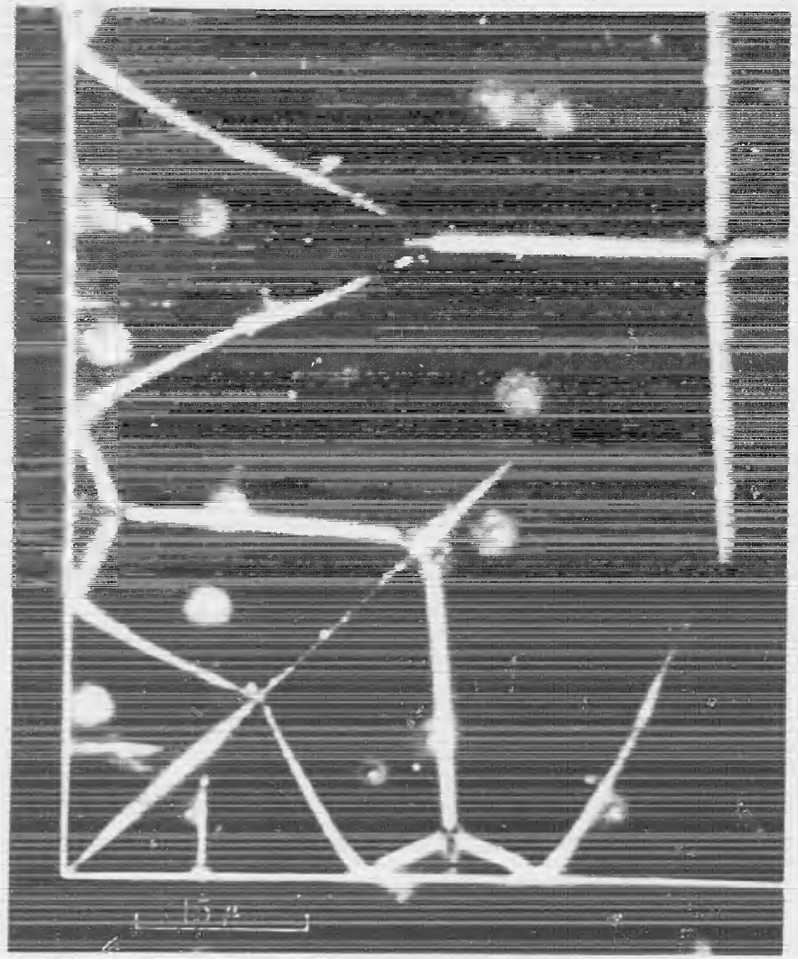

Fig. 12(a) Corner domain structure in a Ni-Fe platelet (81% Ni) with weak negative anisotropy and about zero magnetostriction.

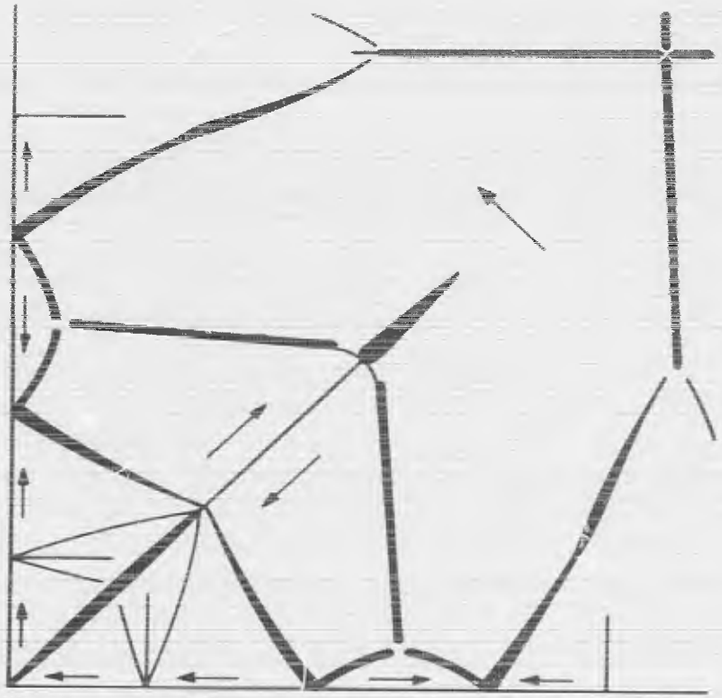

Fig. 12(b) Sketch of (a) indicating how the tulip pattern of Fig. 11(a) generates the corner structure in (a) and the chevron pattern of Fig. 8(a).

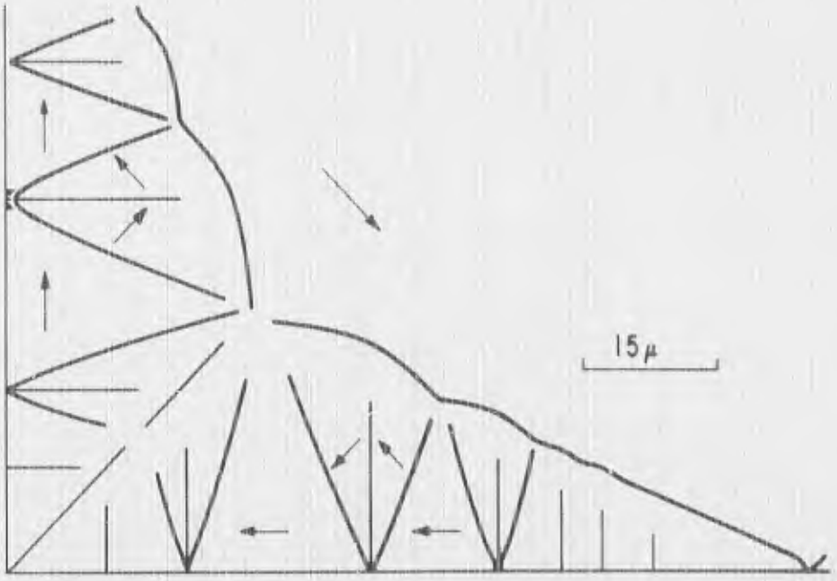


Fig. 13 Sketch of a corner domain structure in the Ni-Fe platelet of Fig. 12 after applying and removing a field. It further illustrates the mode of formation of both chevrons and echelons.

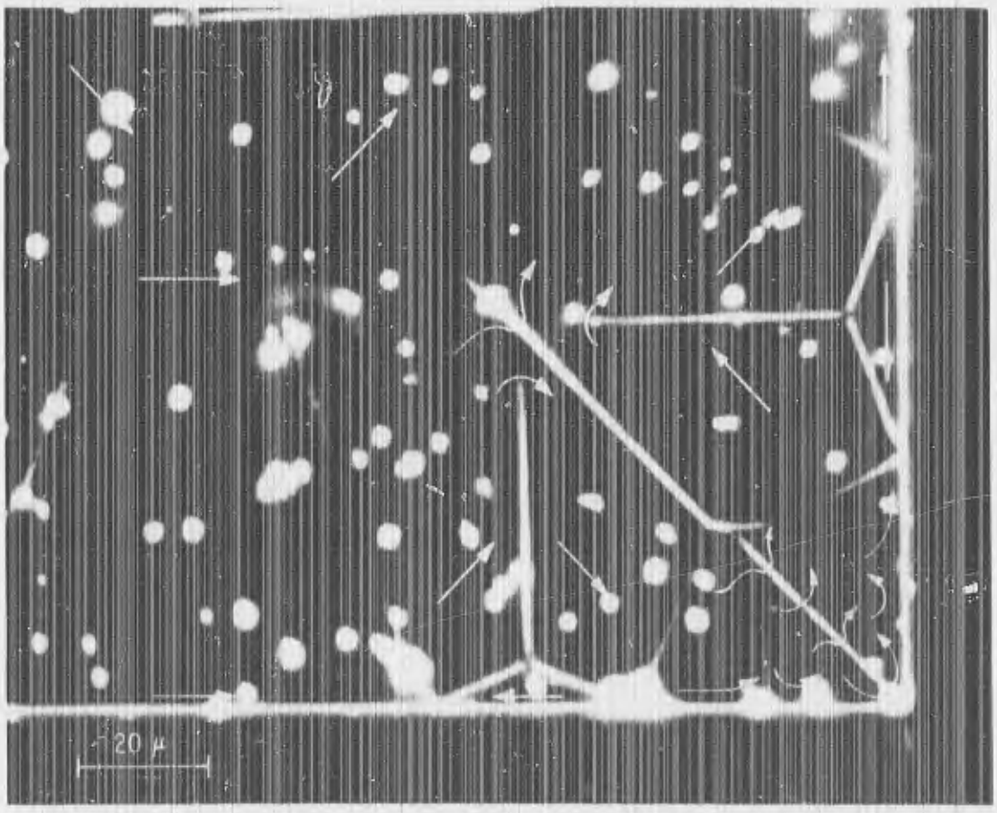


Fig. 14 Corner domain structure similar to that of Fig. 12, but in a Ni-Co platelet with weak negative magnetocrystalline anisotropy and strong negative magnetostriction.

The corner structure of the Ni-Fe platelet of Fig. 12 is closely similar to that of the Ni-Co platelet of Fig. 14. While both platelets have low negative magnetocrystalline anisotropy, the Ni-Co alloy is highly magnetostrictive, while the Ni-Fe platelet is of a composition having about zero magnetostriction. The strains set up by the magnetostrictive changes in length along the directions of magnetization effectively add another anisotropy term. It is probably this magnetostrictive anisotropy that causes the 45° domain walls that converge near the upper left of Fig. 14 to be so even.

A further demonstration of magnetostrictive anisotropy appears in Fig. 15 of a Ni-Co platelet with low negative magnetocrystalline anisotropy. The platelet is stuck to a thin layer of grease. The center of the crossed domain walls is the peak of a raised area of the surface, due to a particle underneath. Therefore the local area is radially strained with the peak as a center. The magnetostrictive constants $\lambda_{100}$ and $\lambda_{111}$ for this platelet ($\approx$20% cobalt) are approximately zero and $-35 \times 10^{-6}$, respectively. Thus, radial strains near the ⟨110⟩ directions tend strongly to align the magnetization perpendicular to these strain directions and along the easy ⟨110⟩ magnetocrystalline direction encompassing the peak. Radial strains near the ⟨100⟩ directions have practically no effect on the direction of magnetization and thus do not tend to broaden the domain walls of the cross. Beyond the strained region the magnetization vector curves more gradually in circling the peak, though in the original negative, magnetostrictively formed 45° domain walls leading from the left tip of the cross to the ends of the faint 180° Bloch wall near the left edge are very faintly visible.

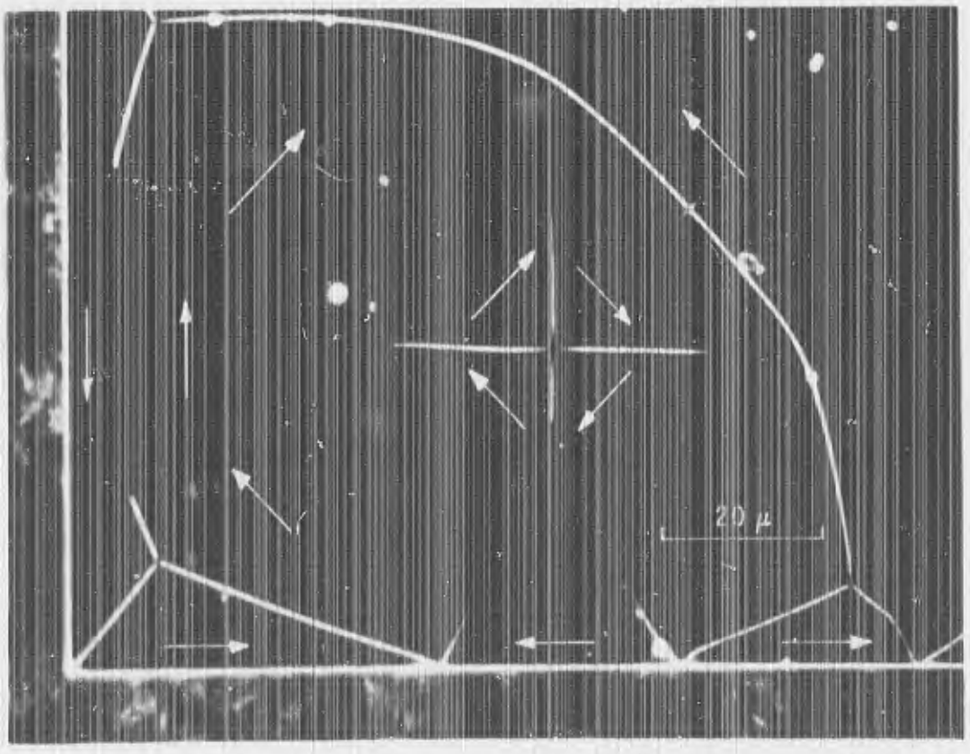


Fig. 15 Domain pattern in a Ni-Co platelet with weak negative anisotropy. The cross centers about a strain peak and is formed because of magnetostriction.

The converse of the above effect, namely, the disappearance of crossed domain walls near a strain peak, was observed to occur in a Ni-Co platelet with weak positive magnetocrystalline anisotropy. For this case the 90° domain walls are rotated 45° with respect to the cross of Fig. 15, while the magnetostrictive constants are both negative. Therefore, the radial strain tends to favor the ⟨110⟩ directions of magnetization at the middle of the domain walls. This broadens the walls in the strained region and makes them too diffuse to collect colloid.

F. Field Induced Stripe Pattern

It will be seen later in the report that nickel platelets about 7500 Å and more in thickness form a stripe pattern because of the component of magnetocrystalline anisotropy perpendicular to the surface. The stripe pattern is not expected to develop in the {100} surfaces of platelets with positive anisotropy (⟨100⟩ easy directions). Figure 16(a) shows the domain pattern in a Ni-Co platelet (≈ 18% Co) with positive anisotropy to the left and negative anisotropy to the right (⟨110⟩ easy planar directions). No stripe pattern is evident in either region. However, a stripe pattern did form in applied fields above about 10 Oe. Figure 16(b) shows the stripe pattern that developed in a longitudinally applied field of 485 Oe. In the region of positive anisotropy to

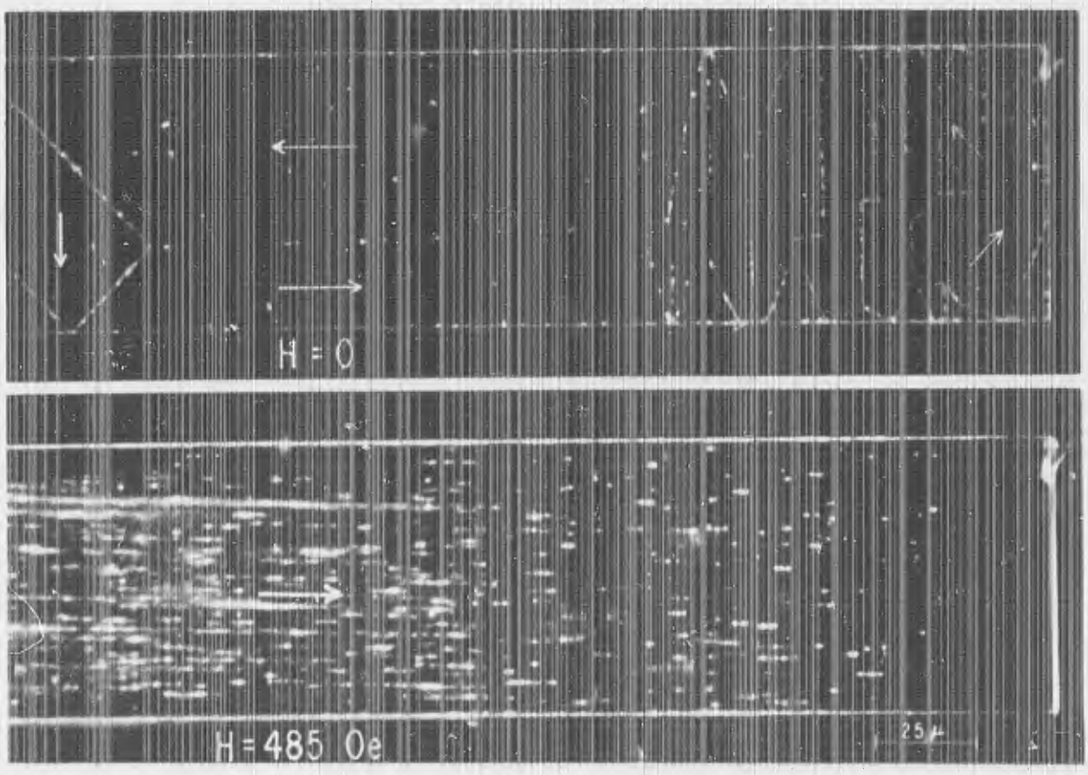


(a)

(b)

Fig. 16 (a) Domain pattern in a Ni-Co platelet with $K_1 > 0$ to the left and $K_1 < 0$ to the right. (b) Stripe pattern that developed in a longitudinal field.

the left, the stripes are more prominent and more widely spaced than in the region of negative anisotropy. The reason why this field induced stripe pattern forms is not presently clear. It may involve nonuniform magnetostrictive strain.[22, 23]

## III. DOMAIN WALL STRUCTURE

### A. Domain Wall Structure vs Platelet Thickness and Composition

Extensive thin-film experimental and theoretical research has centered on domain wall structure as a function of film thickness, composition, growth conditions, and applied field history. [See, for example, reviews by Feldtkeller and Middelhoek.[16, 24, 25]] Figure 17 shows the domain wall energies vs thickness calculated by Middelhoek for 180° walls in Permalloy films.[26] It is seen that Néel walls are energetically favored up to 200 Å, crosstie walls between 200 Å and 1000 Å, and Bloch walls above 1000 Å. The range over which Neel walls are favored increases as the wall angle decreases.

In experimentally observed thin films, the domain wall ranges vary somewhat among various workers, and also the ranges overlap. To what extent this is due to film imperfections and to unknown parameters is not clear. The near perfection of the platelets, plus the knowledge of their physical and ferromagnetic constants, promises to make them excellent specimens for checking theoretical calculations of domain wall ranges and also for determining to what extent the overlapping represents intrinsically allowed metastable structures.

A program to plot out the regions of domain wall type vs thickness and composition is currently under way. This involves using the electron microprobe analyzer with some special computer programs developed by E. Lifshin, the instrument's operator. While the platelet thickness could be measured by light interference techniques before domain observations are made, it is generally more convenient experimentally to observe many platelets and select only those few for thickness and composition determination that show some desired details.

Figure 18 shows two types of 180° domain walls in a nickel platelet 825 Å ± 125 Å thick. The bright wall to the right is a Neel wall. While this wall is of uniform composition, another Neel wall in the same platelet contained several Bloch lines. The double-appearing wall to the left is probably a crosstie wall with a very close and uniform packing of the Bloch lines. This deduction follows from the walls observed in the Ni-Co platelet of Fig. 19. The diagonal 180° wall

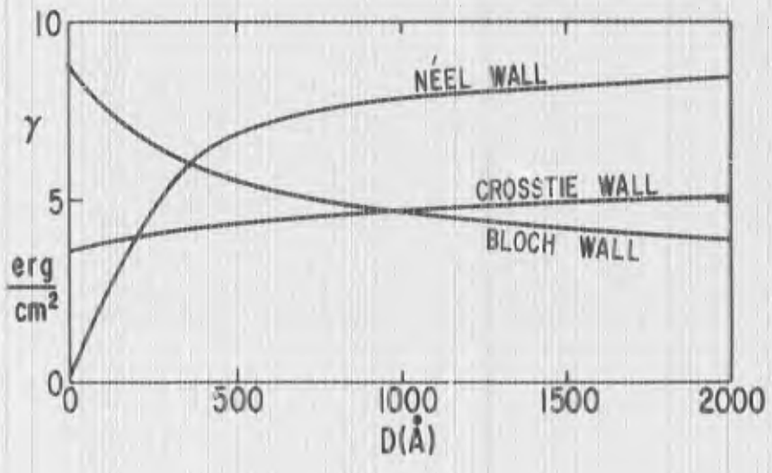


Fig. 17 Calculated domain wall energies vs thickness for 180° walls in Permalloy films (after Middelhoek).

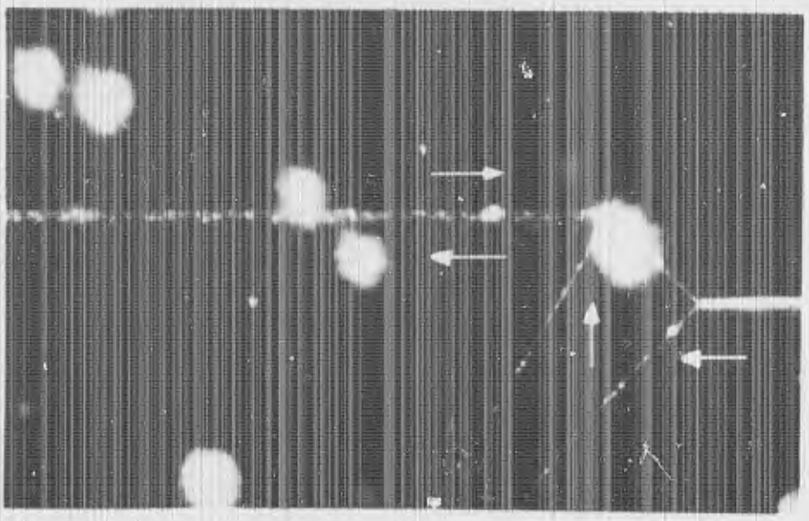

Fig. 18 Two types of 180° walls in a nickel platelet 825 Å thick; a bright Néel wall to the right and a crosstie wall with a close and uniform packing of Bloch lines to the left.

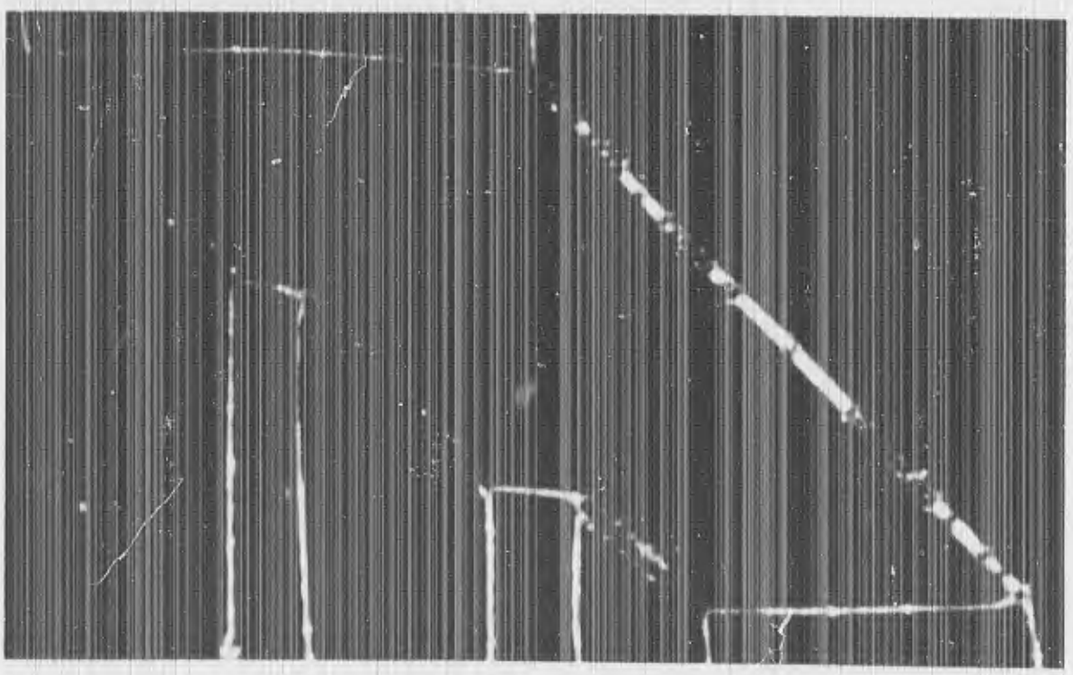

Fig. 19 A Ni-Co platelet with bright 180° Néel wall segments containing widely separated Bloch lines, and a double-appearing 180° wall containing a close but resolvable packing of Bloch lines.

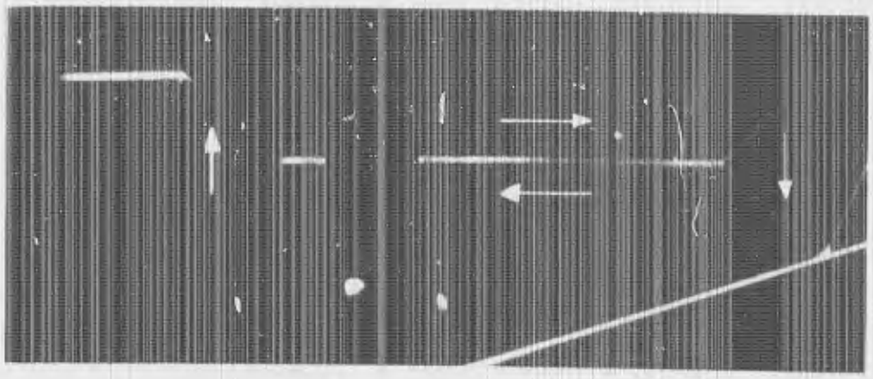

Fig. 20 Three types of 180° walls in a nickel platelet 1300 Å thick; a bright Néel wall to the left, a faint Bloch wall to the left of center, and a crosstie wall to the right.

to the left contains bright Néel wall segments as well as crosstie segments in which the circle and cross Bloch lines are individually resolvable. The double-appearing diagonal walls to the right are similar to the left-hand wall of Fig. 18, but here the individual Bloch lines can be resolved in some regions in the original photograph. It has previously been noted that crosstie walls show up more clearly in Ni-Co platelets than in pure nickel platelets.[1, 2]

Figure 20 shows three types of 180° domain walls in a nickel platelet 1300 Å thick: a bright Néel wall to the left, a faint Bloch wall just to the left of center, and bright Néel wall segments containing Bloch lines, with the line density increasing to the right, so that the region to the right of center may be called a crosstie wall.

Similar details show up somewhat more clearly in the Ni-Co platelet of Figs. 21(a), (b)--(thickness and composition still to be determined). From left to right, the horizontal 180° wall of Fig. 21(a) contains a Bloch line pair [a circle (●) and a cross (x) Bloch line[27]], a faint Bloch wall, a cross Bloch line, a bright Néel wall segment, a circle Bloch line, and another Bloch wall segment. If the left-hand Bloch line is assumed to be pointing upwards (⊙), then the other spin directions are determined in sequence. For example, with the help of the schematic diagram, it may be seen that the spins in the first Bloch wall point upward (⊡) and continue the counterclockwise winding sequence as viewed from left to right, while the spins in the second Bloch wall point downward (⊠) and form a segment that could unwind.

Figure 21(b) developed from Fig. 21(a) after a small field was applied and removed. The central Néel wall segment of Fig. 21(a) has moved to the left and collapsed, and a second Bloch line pair has formed. (This pair formation involves one full rotation of the spins as viewed along the wall as an axis. The alternative scissorlike motion would result in an unwinding, attractive, and, therefore, unstable spin structure.) Intermediate photographs show that only the upper cross Bloch line of the right, vertical 180° domain wall of Fig. 21(a)

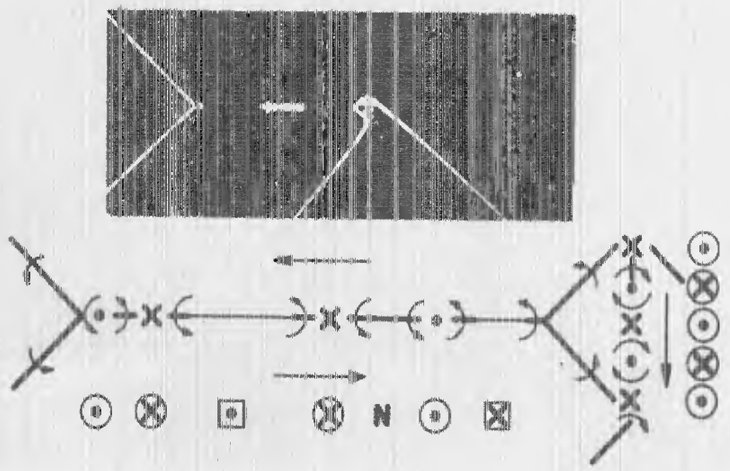

Fig. 21 (a) Two 180° walls in a Ni-Co platelet containing Bloch lines, faint winding and unwinding Bloch walls, and a bright Néel wall. In the sketch below showing the spin directions, ⊙ and x are circle and cross Bloch lines, ——— is a Bloch wall, ▬▬ is a Néel wall, ⊡ and ⊡ represent the spin-up direction, and ⊗ and ⊠ represent the spin-down direction.

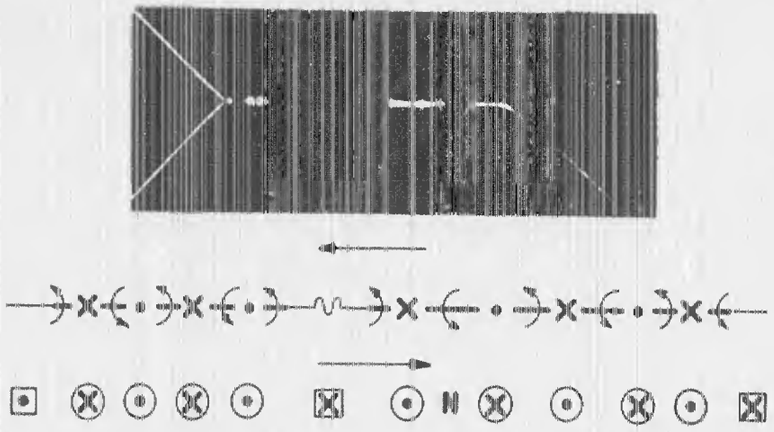

Fig. 21(b) The subsequent structure that developed along the horizontal 180° wall after a small field was applied and removed. Tracing the spin directions indicates that the cross Bloch lines (x) were pointing upward (⊙) in the vertical 180° wall of (a).

remain during the change, to become the left-hand cross Bloch line of the bright central segment in Fig. 21(b), and the neighboring two Bloch line pairs to the right reformed as the domain walls move. But this Bloch line serves to establish, through the adjacent schematic sketches, that the cross Bloch line (x) of the vertical 180° domain wall of Fig. 21(a) points upward (⊙), opposite to those in the horizontal 180° domain wall.

Figures 22(a) and (b) show some further details of domain wall structure in two Ni-Co platelets. The first figure shows some unusually large crossties. The schematic topological structure of the left-hand set is shown in the adjacent

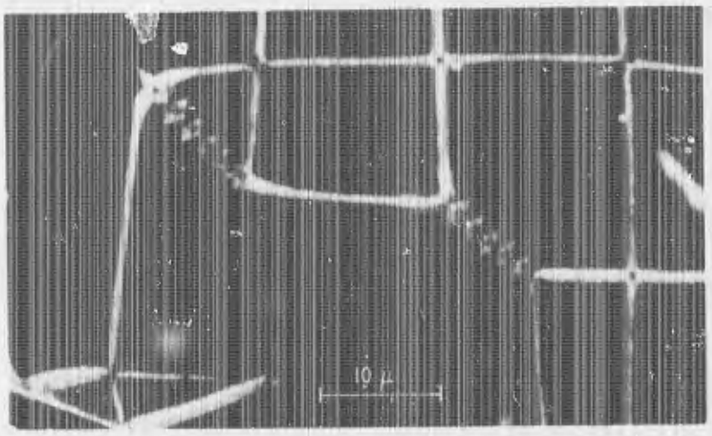


Fig. 22(a) Crosstie walls in a Ni-Co platelet and a schematic diagram representing the left-hand structure. A cross Bloch line lies at the left junction of the 180° and 90° walls.

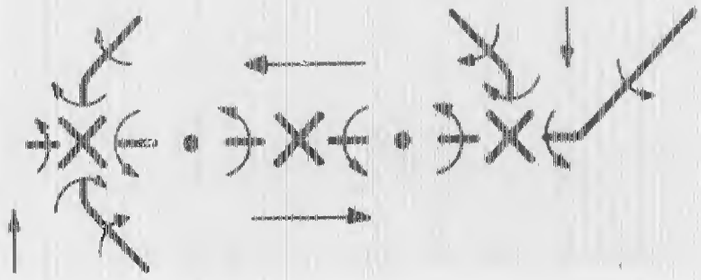

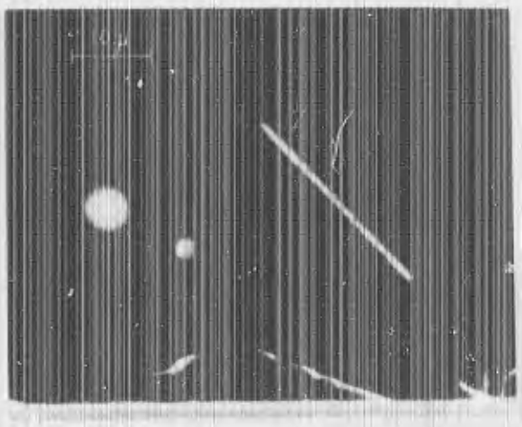

Fig. 22(b) Néel wall with four Bloch-line pairs in a Ni-Co platelet. The schematic diagram indicates that there is no Bloch line at the left junction.

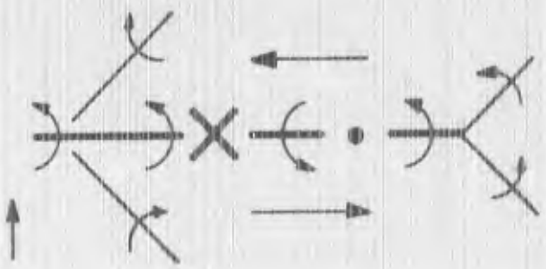

sketch, though the photograph indicates that the actual spin pattern is more complex. A further detail is that a cross Bloch line exists at the left junction of the 90° and 180° walls in Fig. 22(a), while there is no Bloch line at the corresponding junction in Fig. 22(b). Here the Néel wall contains four Bloch line pairs. It need not have contained any, but since it does, then it is clear from the adjacent sketch that the first Bloch line away from the junction must be a cross Bloch line.

Figure 12(a) also shows some details relevant to the discussions of Figs. 22(a) and (b). The lower segment of the diagonal wall starting from the corner is a bright Néel or partially Néel wall and therefore the spin pattern is similar to that at the junction of Fig. 22(b). The upper segment, however, is faint and is therefore a Bloch wall. This makes the far junction a modified form of the cross Bloch line shown at the junction of Fig. 22(a).

Figure 23 shows a peculiar crosstie structure, a giant crosstie spot, in the 180° Néel wall to the right of center. Because it contains five dark spots in a symmetric array, the conjecture was originally made that the structure contained five Bloch lines.[1] This proved to be incorrect,[2] and the actual structure is shown schematically below the photograph. The vertical set of three Bloch lines constitutes a winding, attractive grouping.

Figure 24(a) shows the domain structure that formed at zero field in a nickel platelet 1400 Å thick after application of a 95 Oe field along a diagonal toward the lower left. Both Bloch (faint) and Néel (bright) 180° domain walls may be seen. However, since no crosstie walls were observed in this platelet, it is possible that the bright walls are of a more complex structure than the Néel walls

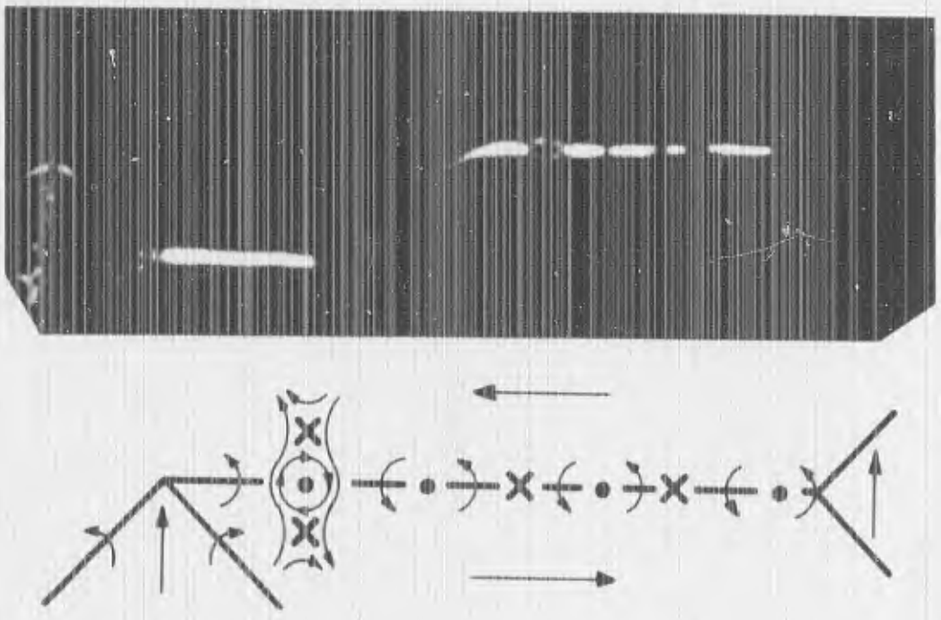

Fig. 23 Néel walls containing a giant crosstie spot (right of center) in a Ni-Co platelet. The schematic diagram indicates that it is formed by a winding Bloch-line triplet.

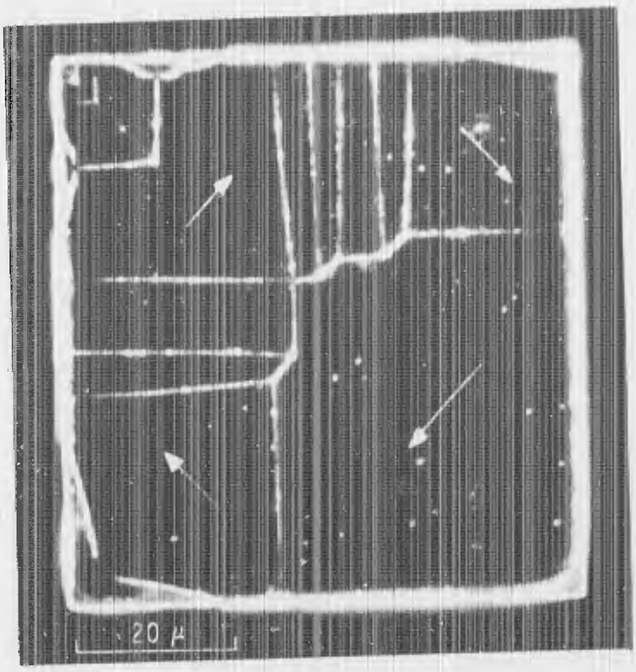


Fig. 24 Domain pattern in a nickel platelet 1400 Å thick. The southeast quadrant is all one domain with high divergence at the edges.

seen in thinner platelets. Notable features of the domain structure are that the southeast quadrant is all one domain, with high divergence of the magnetization at the edges and corner (this causes the band of colloid to collect), and that horn-shaped domains, also with high divergence, exist at two corners. Echelons did subsequently form at the three corners with high divergence when more colloid was added and, presumably, mechanically disturbed the platelet.

Similar horns appear at higher magnification in the 1100 Å thick nickel platelet of Fig. 25. These grew from a nucleus of reverse magnetization at the

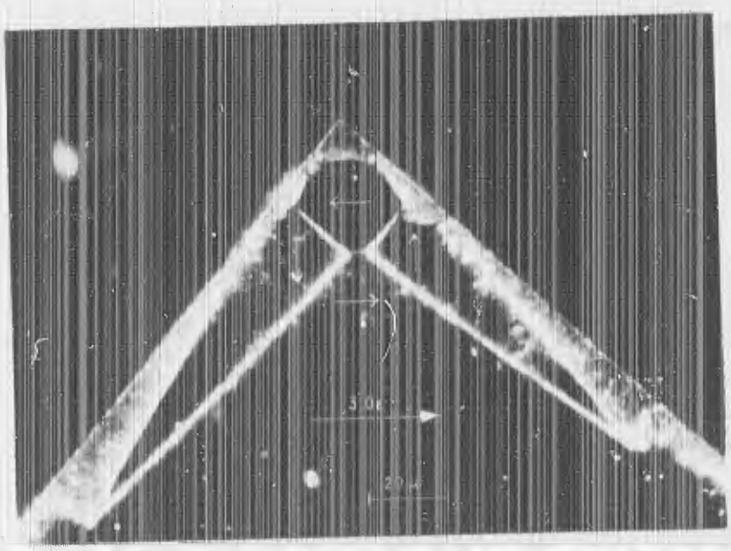

Fig. 25 Horn-shaped domains and high edge divergence at the corner of a nickel platelet 1100 Å thick in a field of 3 Oe to the right. The platelet has a saturation field of 240 Oe and a nucleation field of -22 Oe.

corner as an applied field to the right was reduced from 25 to 3 Oe. The high divergence of the magnetization and the subsequent collection of colloid over extensive areas away from the domain walls result from the gradual spatial rotation of the spins. For example, in the regions near the horn tips the spins rotate from a horizontal direction just to the outer sides of the horns to directions approximately parallel to the edges at the edges. When all domains were driven out of the platelet of Fig. 25 by a field along the diagonal, the platelet remained a single domain specimen until the field was reduced through zero and increased in the reverse direction to 22 Oe. (Saturation and nucleation in platelets are discussed more extensively in Section IV.)

Figure 7 (in Section II) shows the echelon domain structure along a ⟨100⟩ edge of a nickel platelet 2700 Å thick. Most of the 180° walls are Bloch walls (faint); only a couple of bright 180° walls appear near the tip of the echelon. In a thinner nickel platelet, 1800 Å thick, with a similar echelon domain structure, no bright 180° walls appeared in the virgin crystal, though some did appear after a field was applied and removed. In the 3400 Å thick nickel platelet of Fig. 26 there are two bright 180° walls. The horizontal one to the right contains a cross Bloch line. This indicates that the wall is at least partially of Néel type.[2] Thicker platelets up to at least 8000 Å also generally contain both bright and faint 180° walls. (See Figs. 1, 3, and 5 of Ref. 1 and Figs. 5, 6, and 9 of Ref. 2.)

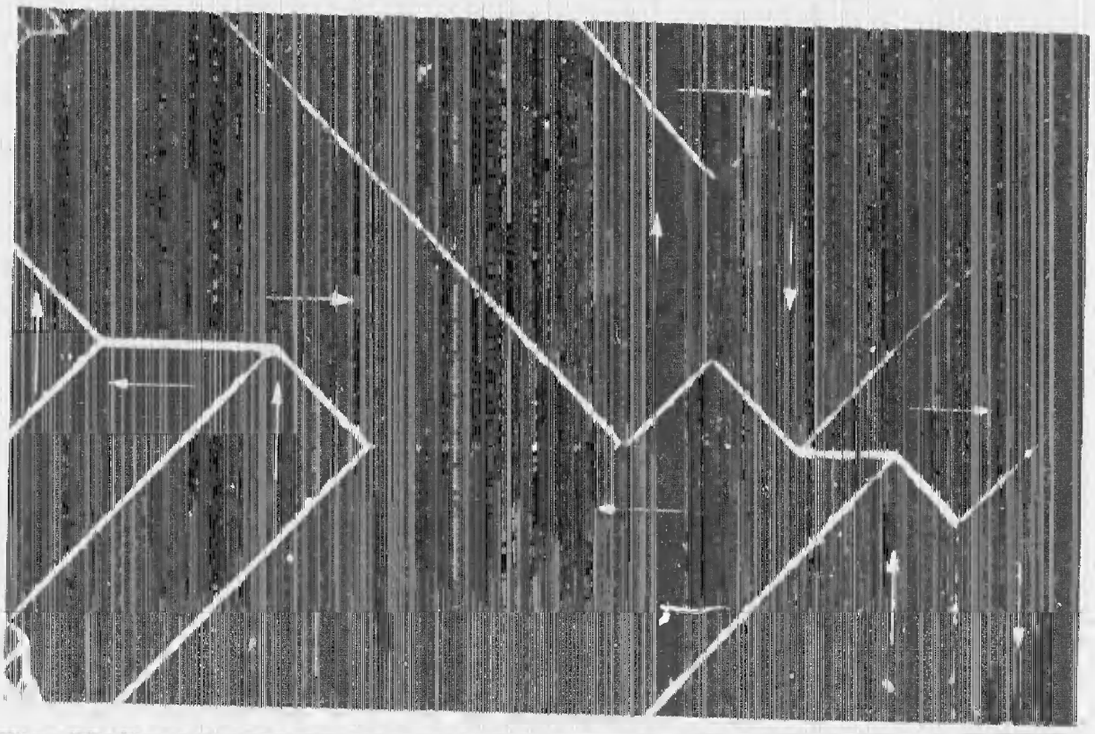

Fig. 26 Domain pattern in a nickel platelet 3400 Å thick. The two bright horizontal 180° walls are intermediate ones of mixed Néel-Bloch character.

The presence of bright 180° domain walls that are at least partially of Néel type in thick platelets presents a structural puzzle since pure Néel walls are calculated to be energetically favored only up to about 200 Å.[26] This, plus the gap from about 1800 Å to 2700 Å, where bright 180° walls are absent or scarce, suggests that the bright walls observed in the thicker platelets are of mixed Néel-Bloch character. Shortly after these walls were first observed,[28] Torok et al.[29] coincidentally presented computer calculations indicating that a domain wall intermediate in structure between Bloch and Néel walls could exist. However, their calculations appear not to pertain to the bright 180° wall, but rather to the nature of the faint Bloch wall, since, for one thing, they show that the Néel to Bloch transition is gradual, whereas what is observed are two kinds of coexisting walls which may be gently moved and rotated in an applied field without loss of identity. Also, they show that all Bloch walls that are not exactly 180° walls much be of intermediate structure. What is observed is that the bright 180° wall is metastable; with a moderate disturbance it will often snap into a faint wall, but the reverse never happens. Therefore, it may be that the faint Bloch wall actually has an intermediate structure, in accord with their calculations, but, if so, this structure would appear to be quite distinct from the intermediate structure of the bright 180° wall.

Figure 27 shows the domain pattern in a nickel platelet 7500 Å thick. Within each domain one may observe faint stripes running parallel to the magnetization. Similar stripes were first observed in thin films by Spain[30] and by Saito et al.[31] Along each stripe the magnetization is pointing out of or into

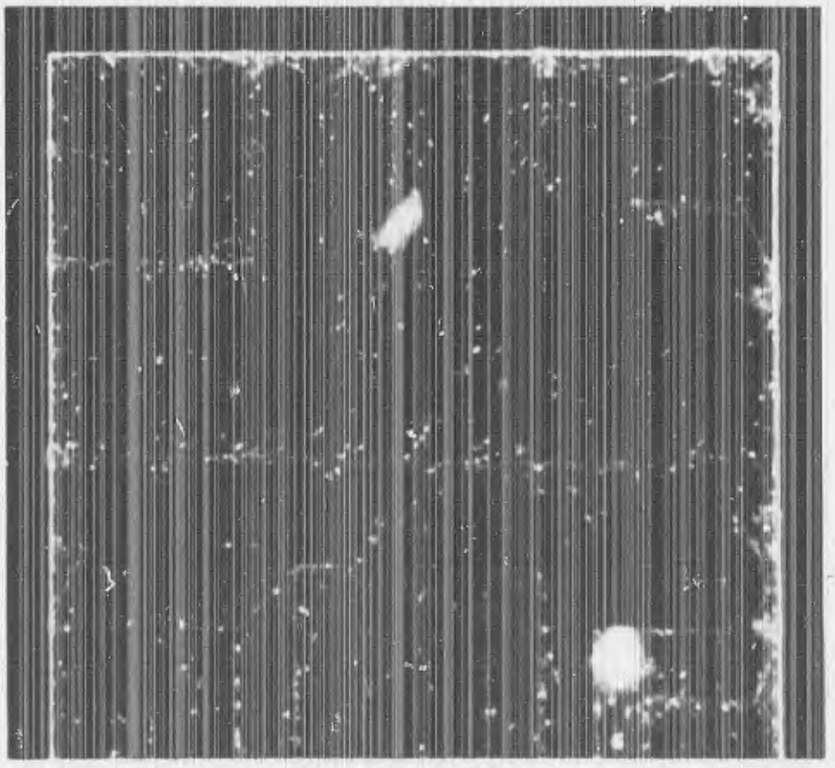

Fig. 27 Domain pattern in a nickel platelet 7500 Å thick, containing a faint stripe pattern.

the plane at roughly a 30° angle. The stripes occur in sufficiently thick specimens with an anisotropy component perpendicular to the surface. [In nickel the ⟨111⟩ directions pointing 35.3° out of the (001) plane of the platelet are the directions of minimum magnetocrystalline anisotropy energy.] The existence of such stripes had been predicted earlier by Kaczér et al.[32] Reference 1 contains further examples of the stripe pattern in nickel and cobalt platelets and some rough quantitative checks on the theories of Kaczér et al.[32] and Saito et al.[31] The stripe pattern is of active current interest, both experimental[33-36] and theoretical.[37, 38] The experimental interest is due in part to their use for magneto-optical display and to their being the cause for "rotatable anisotropy" in thin films. For the theorist the stripe pattern represents a neat and challenging problem in micromagnetics.

## IV. DOUBLE WALLS

### A. Introduction

Ferromagnetic domain walls that are made to approach each other may interact to form double walls. Williams and Sherwood first observed such behavior in thin (50 Å to 200 Å) vacuum deposited films.[39] Paulus has also observed double walls in a single crystal of nickel ferrite,[40] and several workers have made further observations on vacuum deposited films.[41-45] Figure 28 shows schematically the possible types of 180° Bloch (a, b) and Néel (c, d) double walls. Type a, for example, is attractive and winding, i. e., the polarities on each surface are opposite, and the sense of spin rotation in both walls is the same. Therefore, a moderate field applied opposite the magnetization between the walls would squeeze the walls closer together, against exchange forces, but should not annihilate it.

Kaczér[46] developed a theoretical explanation for the double walls observed by Williams and Sherwood, in which he derived an energy expression

$$E = \pm 16\gamma_0 te^{-\sigma} \mp 2\pi M_S^2 t^2 \sigma^{-2} - 2M_S Ht \sigma \delta_0 \qquad (2)$$

where E is the energy per unit length of wall; $\gamma_0$ is the domain-wall energy parameter $(AK)^{1/2}$; t is the film thickness; $\sigma$ is the distance between walls divided by the domain-wall thickness parameter $\delta_0 (\equiv (A/K)^{1/2})$; and H is the applied field. The terms of the equation represent interaction, dipole-dipole, and external field energies, respectively. Using this equation, Kaczér found a wall separation at equilibrium of about 0. 5 μm, compared to the observed value of about 4 μm, and a critical field of 0. 85 Oe for causing the walls to move apart, compared to the observed 2 Oe.

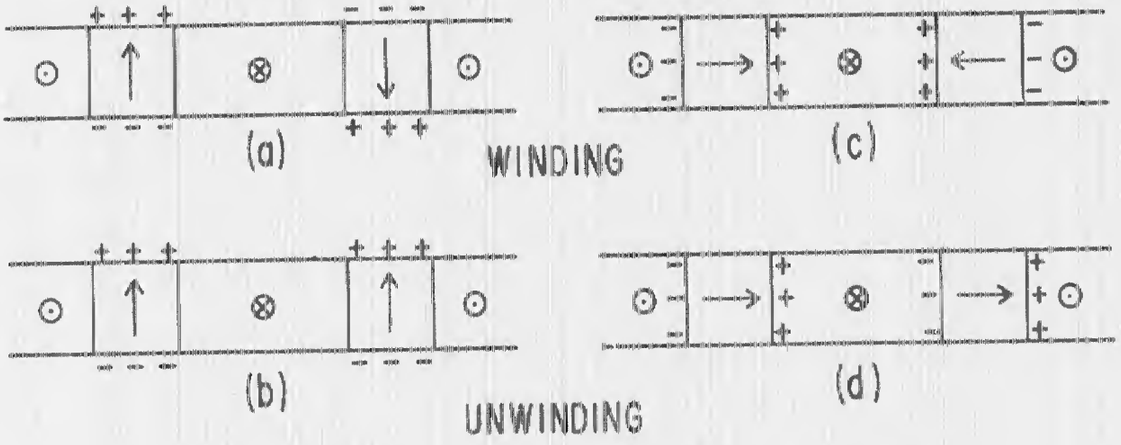


Fig. 28 Diagram of four types of interacting 180° domain walls; (a) and (b) represent winding and unwinding Bloch wall pairs, respectively; (c) and (d) represent winding and unwinding Néel pairs, respectively.

Williams and Sherwood mentioned in their paper that the application of a field normal to the 147 Å thick film caused a concentration of colloidal magnetite on one wall and a deficit on the other. This indicates that the double walls consisted of winding Bloch pairs [Fig. 28(a)] and Kaczér's numerical calculations are for this case. However, Behringer[47] pointed out that very thin walls (50 Å) should be Néel walls, and also that Kaczér's analysis was somewhat inconsistent in dealing with Néel walls and with the anisotropy constant K. He also suggested that the 147 Å thick film of Williams and Sherwood might have some three-dimensional form intermediate between a Bloch wall and a Néel wall. Subsequent analysis by Middelhoek[16] indicates that even the 147 Å thick film should have only Néel walls. If this is so, then the above observation regarding the colloidal concentration presents a puzzle. Perhaps current calculations with the use of a computer on the structures of Néel, Bloch, and intermediate walls will resolve it.[29, 48-51] In any case the order of magnitude disparity between theory and experiment suggests a need both for improved theories and for less imperfect experimental specimens. Since platelets are nearly perfect specimens and, since a variety of double walls are observed in them, the need has now been resolved to that of developing theories that adequately accord with experimental observation. An adequate theory that is tractable to computation should, of course, yield significant information on domain wall structure and interaction.

B. Double 90° Walls

Figure 29(a) shows the domain structure in a 3600 Å thick nickel right-triangular platelet in an 8 Oe field applied along one of the easy ⟨110⟩ directions, perpendicular to the hypotenuse. The upper pair of 90° domain walls has joined at the center to form a stable double wall. Figure 29(b) shows a similar double wall in the same platelet at higher magnification. The walls are observed to snap together when the bowed sections approach within about 1 μm of each other, to form the 0.7 μm wide double wall shown. The applied field must be reduced by about 0.35 Oe for the walls to snap apart (to 1.4 μm separation). A more significant measure of this hysteresis cycle should be the radii of curvature of the domain walls just before and after snapping together and apart, since we have seen from Eq. (1a) that these give the net effective fields acting along the walls, in the approximation that we neglect the free poles arising from lack of continuity of the normal component of magnetization across the walls. The net field given by Eq. (1a) for the pair below the double wall of Fig. 29(b) is about 0.003 Oe for $\gamma_{90} \approx 0.2$ erg/cm$^2$, $M_S = 484$ emu, and $r = 1.2$ mm. Thus the applied field of 10 Oe is highly shielded from the interior by demagnetizing fields arising from magnetic pole formation along the edges and along the curved domain walls. Determination of the changes in $H_r$ when the walls snap together and apart will require more accurate radius measurement techniques than are presently in use. Calculating the correct forms for Eqs. (1a) and (1b), with divergence of the magnetization included, is also a problem for the future.

Figures 30(a) and (b) show double 90° walls in a right-triangular nickel platelet about 7000 Å thick. The structures and interactions are now clearly quite complex. The platelet does show a faint stripe pattern, owing to its thickness and its negative magnetocrystalline anisotropy. The periodicity of this pattern continues into the double wall region.

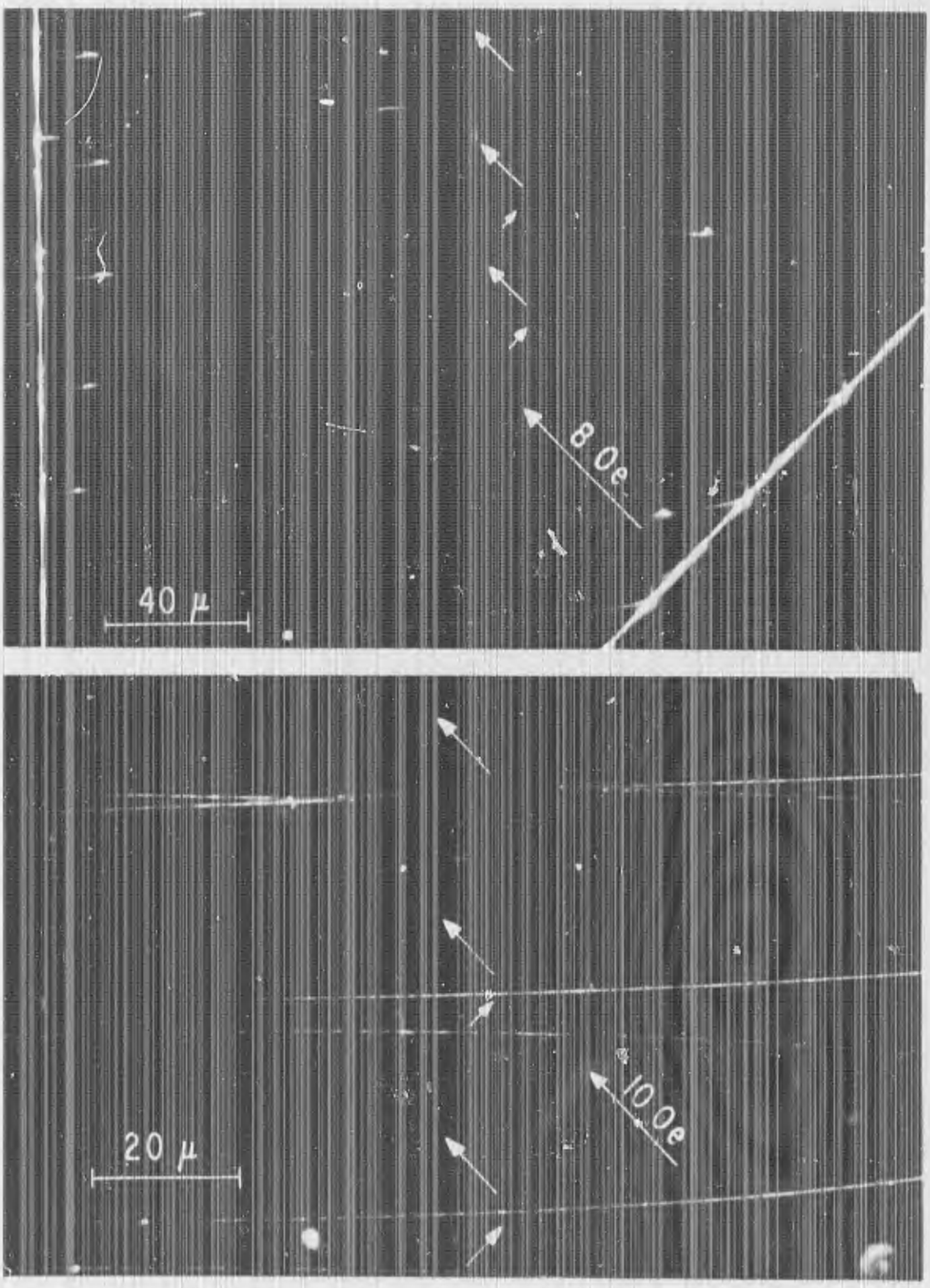


Fig. 29 (a) Domain structure in a 3600 Å thick nickel platelet in an 8 Oe ⟨110⟩ field. The upper pair of 90° walls has joined at the center to form a stable double wall. (b) A similar double wall in the same platelet at higher magnification.

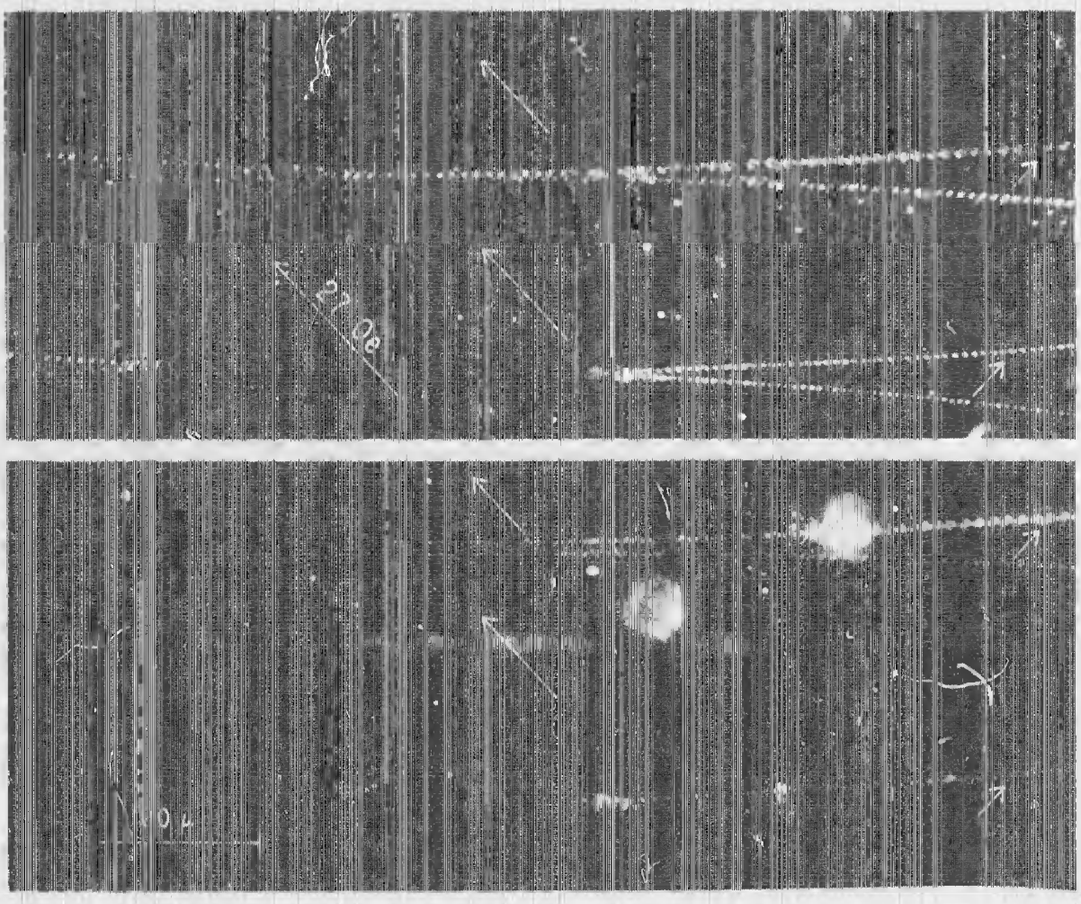


Fig. 30 (a) A complex double 90° wall in a nickel platelet 7000 Å thick in a 27 Oe ⟨110⟩ field. (b) Two interacting 90° walls in the same platelet (a different pair in a field of 22 Oe).

This same platelet showed the unusual 90° walls of Fig. 31 in zero field, where the walls display two lines, one bright, the other faint, and the lines may exchange positions here and there along a wall. Thus, even the 90° wall may have a complex, asymmetric structure in the platelet. When two such walls are brought together to form a double 90° wall, as in the previous figures, the two nearer lines merge to form a three-line double wall. While it is unlikely that the structures observed in this thick platelet will be analyzed in the near future, their appearance shows that regularity may occur in much more complex structures than have previously been considered. It is also to be noted that Kaczér predicts a critical thickness, above which double Bloch walls should not exist.[46] For nickel this is only 890 Å if the wall thickness parameter, $\delta_0$ is taken as 260 Å.

C. Double 180° Walls

Figure 32 shows a double 180° wall in a Ni-Co platelet 230 μm wide, in a 9 Oe applied field. (The thickness is still to be measured.) This arrangement, with the field parallel to the magnetization in the expanding domains, is that considered in the theories on double walls. The structure probably consists of winding Bloch walls [Fig. 26(a)]. For this geometry and for a 180° wall, Eq. (1b) gives a net field of 0.01

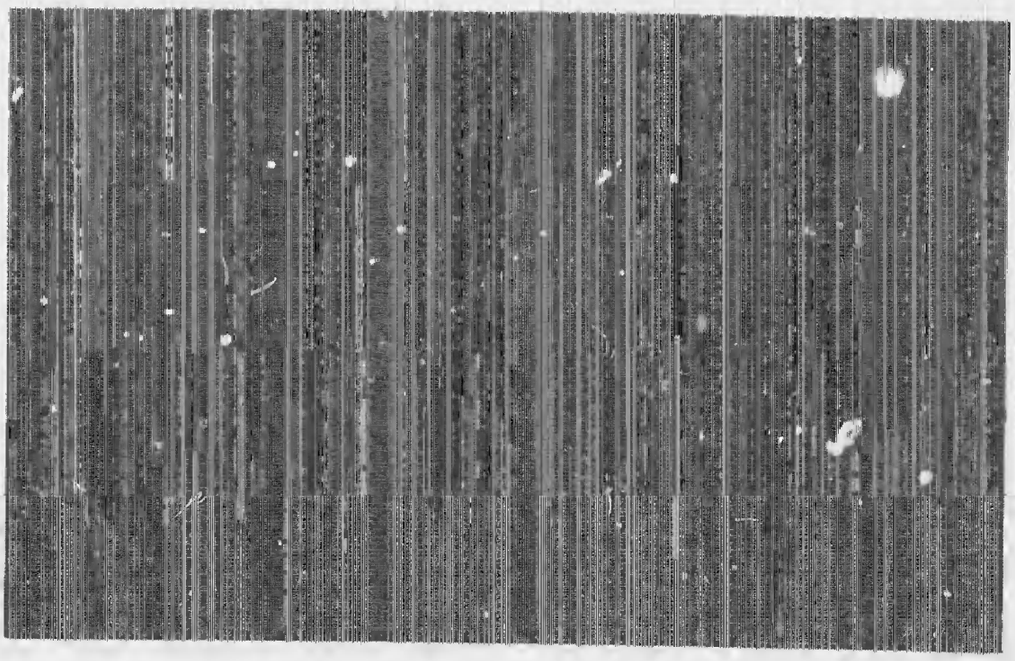

Fig. 31 Double-appearing 90° walls in the platelet of Fig. 30 in zero field. The bright line jogs here and there from one side of the wall to the other.

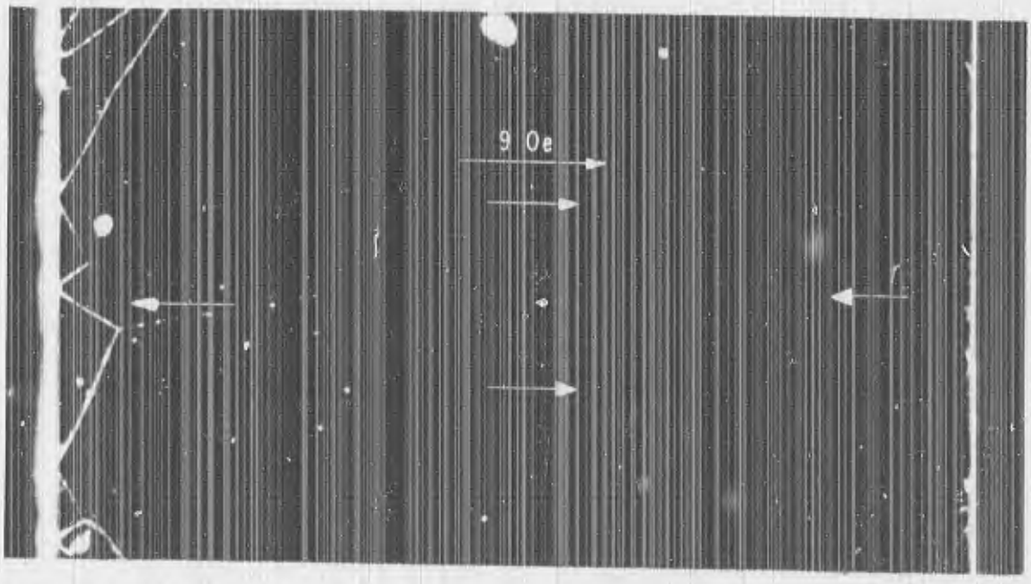


Fig. 32 Double 180° wall in a Ni-Co platelet in a 9 Oe field perpendicular to the edges.

Oe acting on the curved wall (for $\gamma \approx 0.2$ erg/cm$^2$, $r \approx 300$ μm, and $M_s \approx 600$ emu). This result, like the previous ones, may be considerably modified when the effects of magnetic charges in the curved walls are accounted for.

By use of Eq. (2), Kaczér predicts a critical field for the separation of the double walls and an equilibrium separation in zero field. These are found very approximately to be ≈ 1 Oe and 1000 Å, respectively, for the Ni-Co platelet. These values are to be compared with $H \approx 0.01$ Oe calculated above and with an observed separation near 7000 Å.

Figure 33(a) shows another double 180° wall at the center of a Ni-Co platelet with positive magnetocrystalline anisotropy. It developed as an off-diagonal applied field was reduced to 15.2 Oe and the two central 90° domain walls of a zigzag domain pattern similar to that of Fig. 33(b) came together. At a lower field of 11.4 Oe the walls separated to form the domain structure shown in Fig. 33(c). This structure provides a further indication that the magnetization between the double walls twists to a direction antiparallel to the magnetization on either side of the double walls. It also helps to indicate that the double wall consists of a winding Bloch pair [Fig. 28(a)]. Figure 33(d) was taken immediately after Fig. 33(a) and at the same field. The change in structure after the spontaneous break-up of the double wall might serve as some indication of the energy contained in the double wall or of the potential barrier against its dissolution.

Figure 34 shows still another double 180° wall near the center of a Ni-Co platelet, but this one is very significantly different from the previous ones. First, the applied field of 4.7 Oe is perpendicular to the walls. Second, the walls are not Bloch walls, since 180° Bloch walls show up quite faintly. (Such a faint 180° Bloch wall separates the two vertically magnetized domains at the right.) Third, the walls are not Néel walls, since continuity with the adjoining 90° walls would then require them to be both attractive and unwinding, and they would annihilate each other. [This also follows from the spike structure, which is similar to that of Fig. 22(b).] One may therefore deduce that they are intermediate walls of mixed Néel-Bloch character. It has previously been deduced that the bright 180° walls were at least partially of Néel wall character.[2] Figure 34 now demonstrates that they are not pure Néel walls. The Bloch components of the double wall may be of the form shown in Fig. 28(b) since the double wall is repulsive in behavior.

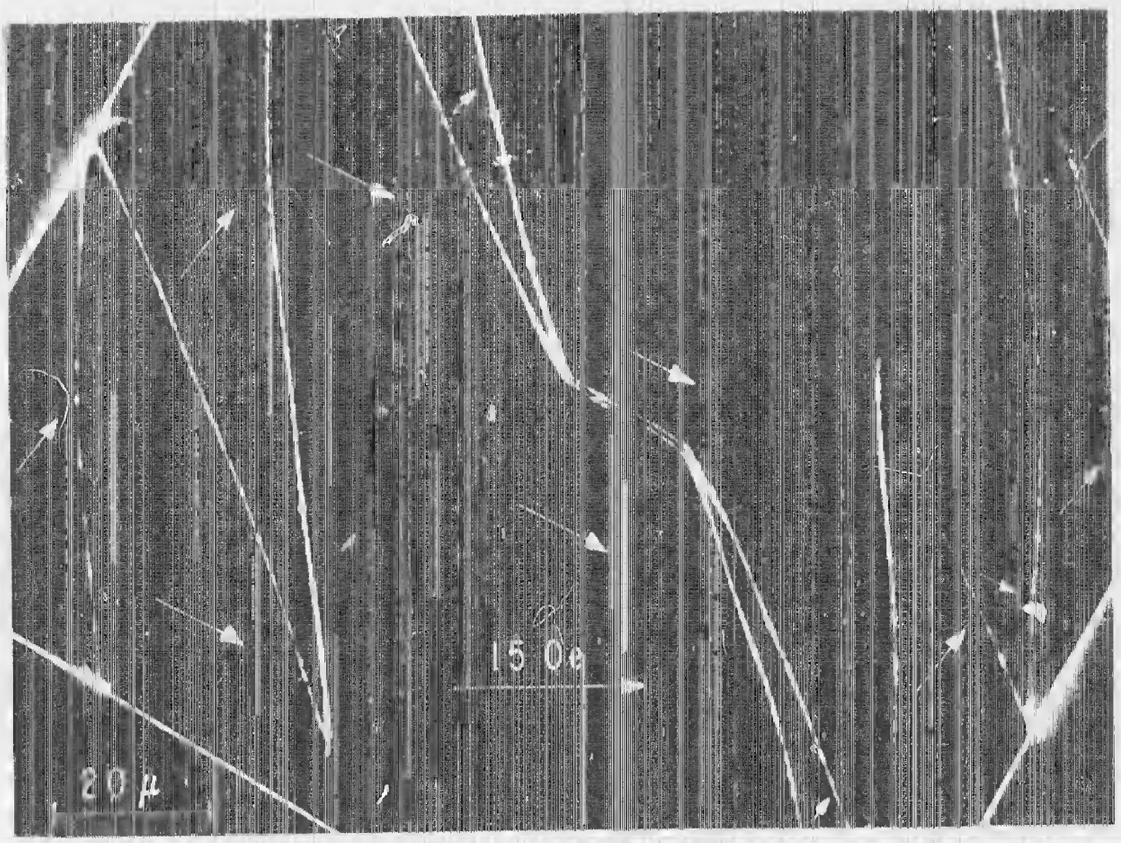


Fig. 33 (a) Double 180° wall at the center of a Ni-Co platelet in an off-diagonal field of 15.2 Oe.

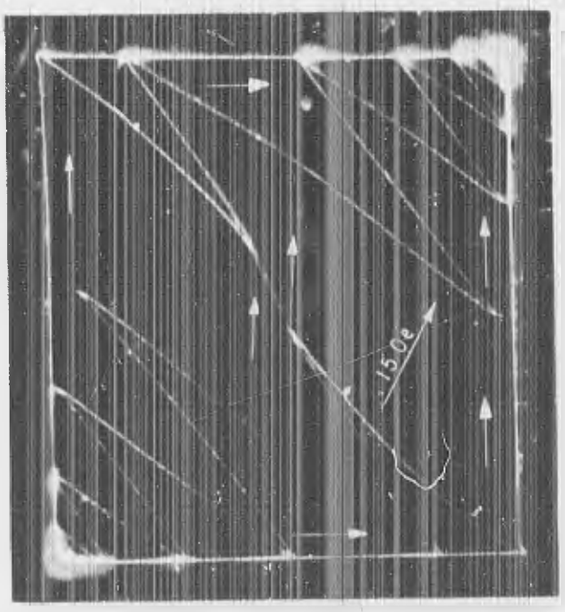


Fig. 33 (b) Zigzag domain pattern in the same platelet in an off-diagonal field of 15.3 Oe. The double wall of (a) developed from a similar pattern as the field was reduced and the two central domain walls came together.

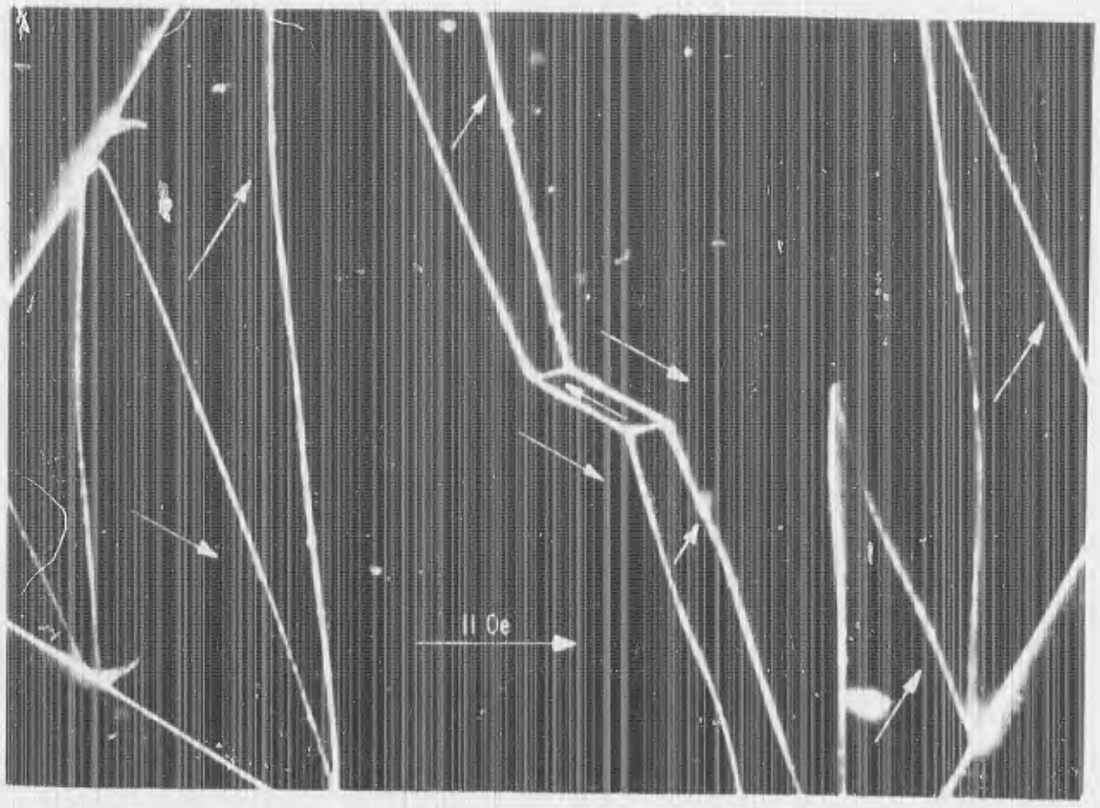


Fig. 33 (c) Structure formed on separation of double walls of (a) in a reduced field of 11.4 Oe.

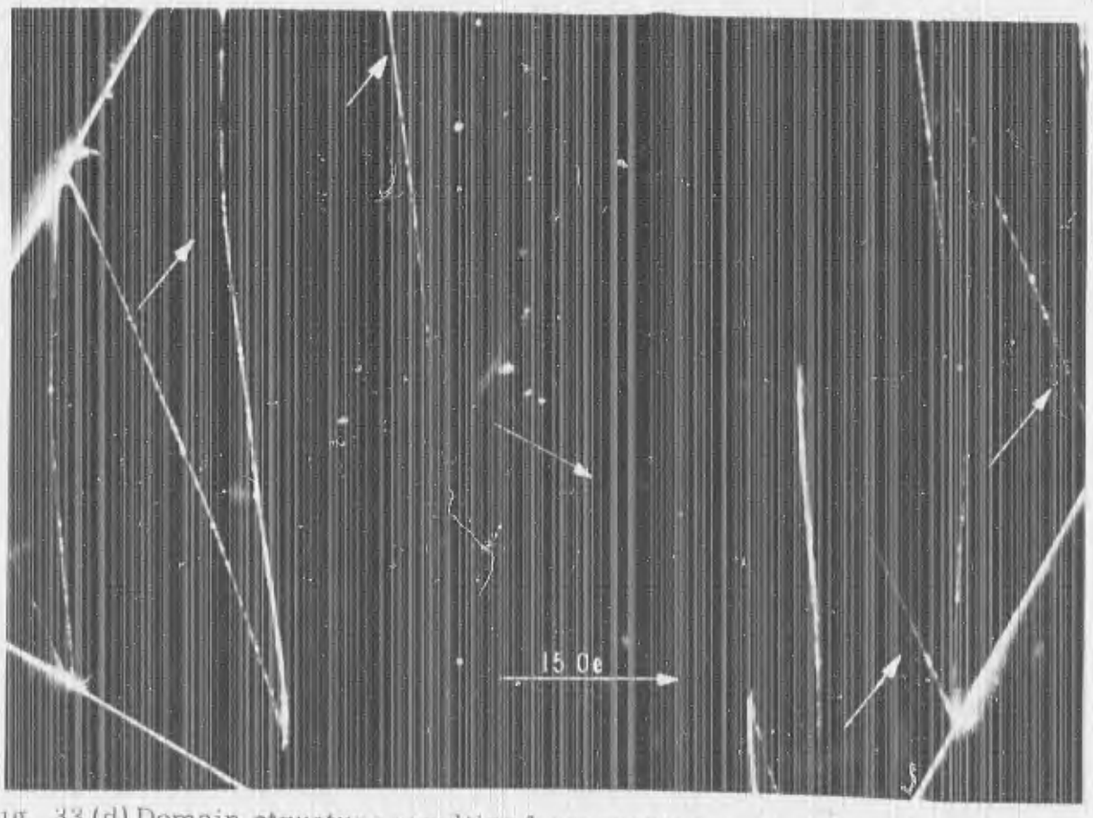


Fig. 33 (d) Domain structure resulting from spontaneous breakup of double wall of (a) at same field.

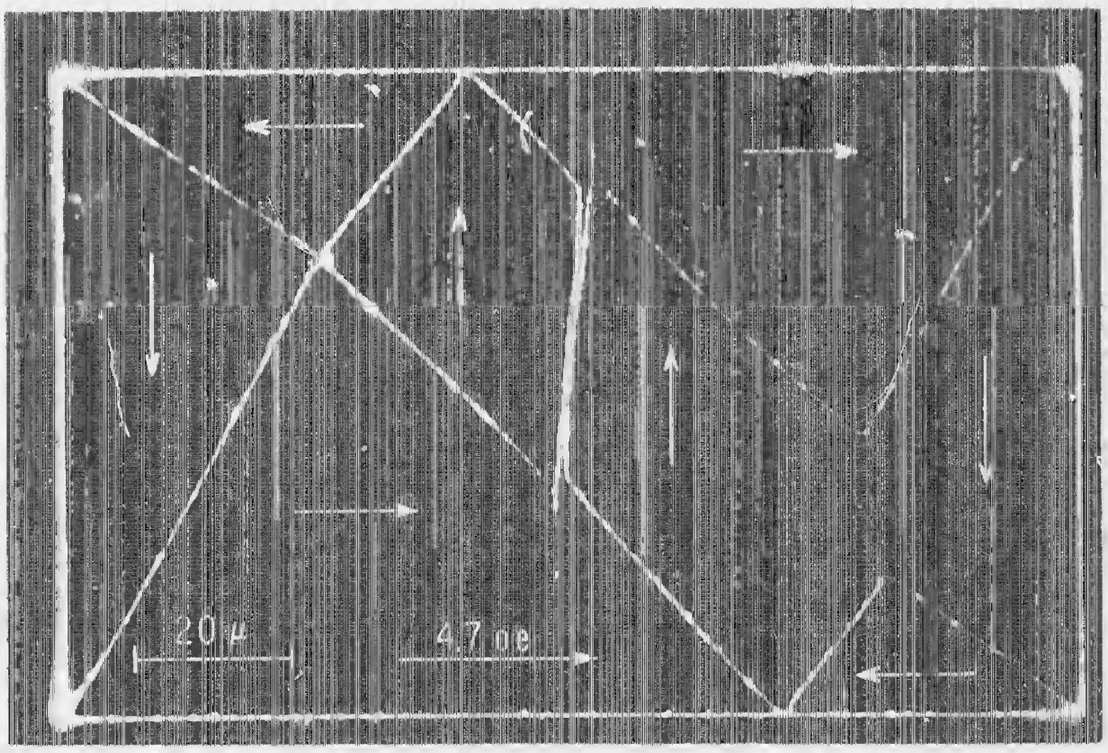


Fig. 34 Double 180° wall in a Ni-Co platelet in a 4.7 Oe field perpendicular to the walls. The individual walls of the pair are neither Bloch nor Néel walls but are of mixed structure.

BLANK PAGE

## V. SATURATION AND NUCLEATION IN PLATELETS

A fundamental assumption of ferromagnetic nucleation theory is that the specimen starts from complete saturation.[52, 53] But the question of whether or not all nuclei of reverse magnetization have been driven out in any given experiment can be a bothersome one. For example, Fowler et al.[54] have observed reverse domains still persisting at the end of a sharp-cornered iron whisker in fields up to 6000 Oe, well above the field at which the crystal would normally be considered as saturated. Other workers have observed sharp changes in domain behavior in several kinds of specimens after fields were applied that were apparently high enough to drive out all nuclei.[55-60]

With nickel and Ni-Co platelets it is now possible to determine the saturation fields quite accurately at geometrically specific sites, namely, at the corners, where boundary conditions should be analytically tractable. This determination is possible through noting the domain configuration that forms as the applied field is reduced. For thin platelets the consequent nucleation field may also be observed.

The clue to determining whether or not saturation occurs at the corner of a nickel platelet in an applied field of several hundred oersteds is contained in Figs. 8(a) and (b) of Section II. (See also Fig. 9 of Ref. 2.) At the high field any nucleus of reverse magnetization will have shrunk to invisibly small size at one of the corners along the diagonal perpendicular to the diagonally applied field. For Fig. 8(a) the magnetization was observed originally to curve around the corner in a counterclockwise direction. A field of 397 Oe was then applied toward the upper left and reduced to 10 Oe to reveal the resulting corner domain pattern. One may trace the magnetization directions in Fig. 8(a) to the corner to show that the magnetization now curves around it in a clockwise direction, i.e., the 397 Oe was sufficiently large to drive out the original nucleus. Now a field of only 356 Oe was applied to the lower right and reduced to 10 Oe to form the domain pattern of Fig. 8(b). Since the magnetization at the corner still curves clockwise, opposite the applied field direction, 356 Oe was not large enough to drive out the nucleus. Further testing narrowed the saturation field, $H_S$, to 364 ± 8 Oe; at the opposite corner it was 398 ± 2 Oe. The platelet is 840 μm square; its thickness is still to be measured. Another similar nickel platelet, 2100 Å thick, had saturation fields of 365 ± 5 Oe, 370 ± 5 Oe, and 405 ± 5 Oe at three of its corners, respectively. If it should turn out theoretically that an atomically perfect corner has a maximum saturation field compared to slightly rounded corners (where the edge radius is larger than one atomic radius), then a large number of such statistics of $H_S$ vs thickness should indicate to a useful degree of accuracy what the ideal values of $H_S$ vs thickness are.

If the platelet thickness is less than approximately 2000 Å, then nucleation and in some cases even saturation may be observed directly. Figure 35(a) shows a nickel platelet (106 by 117 μm on a side and 1100 Å thick) in a diagonal field of 15 Oe to the lower left. The platelet had been saturated in a field of about 240 Oe applied toward the upper right, and this was reduced through zero to the -15 Oe shown. The magnetization is still directed toward the upper right. The bands of colloid inside the platelet edges show the strong divergence of the

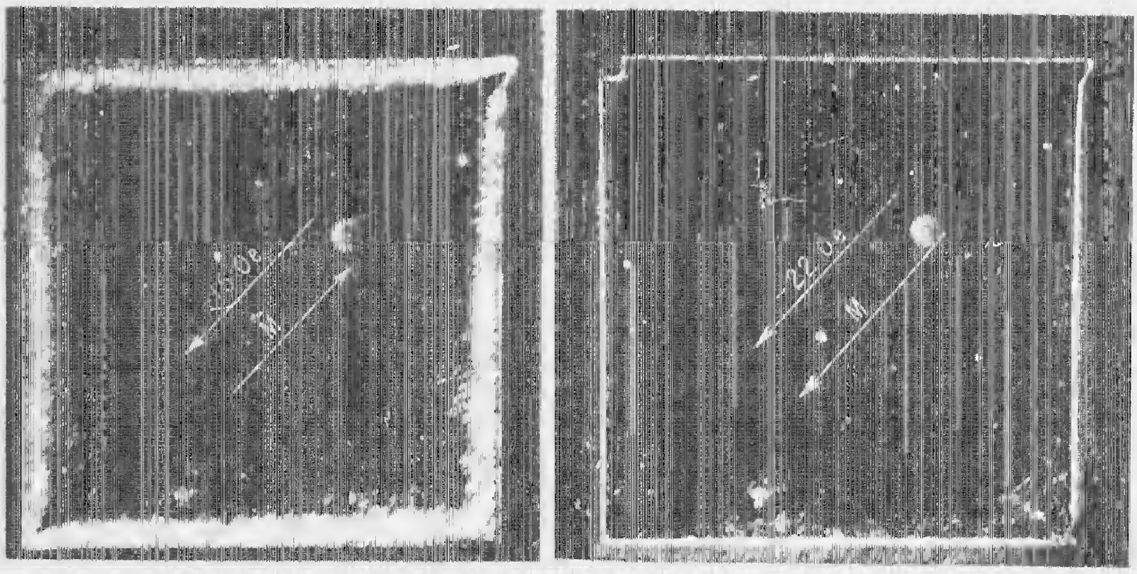

(a) (b)

Fig. 35 (a) Single-domain nickel platelet, 1100 Å thick, in a negative diagonal field of 15 Oe. The internal band of colloid indicates high divergence near the edges. (b) Same platelet after nucleation at -22 Oe.

magnetization as it rotates from being approximately parallel to the edges at the edges to being antiparallel to the field in the interior regions. It is not until the field reaches -22 Oe, in Fig. 35b, that nucleation occurs (possibly at the lower right corner, since there is some domain structure visible at the opposite corner) and reversal of magnetization takes place. Figure 25 shows a corner of the same platelet after a pair of horn-shaped nuclei of reverse magnetization--the form that usually developed after nucleation--was allowed to expand in a reduced field of 3 Oe.

Figure 36 shows a nucleus of reverse magnetization at the corner of a Ni-Fe platelet in a diagonal field of 16 Oe. (It is the same low-negative-anisotropy platelet as that of Fig. 12.) For this case the field at saturation could be directly observed to be 65 Oe. As the field increased, the two outer domain walls forming the sides of a shield squeezed closer together but were still resolvable up to the saturation field, when they snapped together to form a single line. As before, the form of the corner domain structure at reduced field was used to check on whether or not saturation had actually taken place.

Saturation fields may be determined at the corners of platelets with positive anisotropy in a manner indicated in Fig. 37. In zero field the end of a long, narrow platelet (specificially, that of Figs. 10 and 11 of Ref. 2, which is 35 μm wide) will have the closure pattern sketched in Fig. 37(a) since the easy directions of magnetization are parallel to the ⟨100⟩ edges. As a field is applied to the right, the 180° wall moves up, bows into a circular arc, and finally snaps out to leave the pattern sketched in Fig. 37(b). Note that the magnetization in the domain at the right edge is directed upward. If a large field with a slight downward component is now applied to the right and suffices to saturate the specimen,

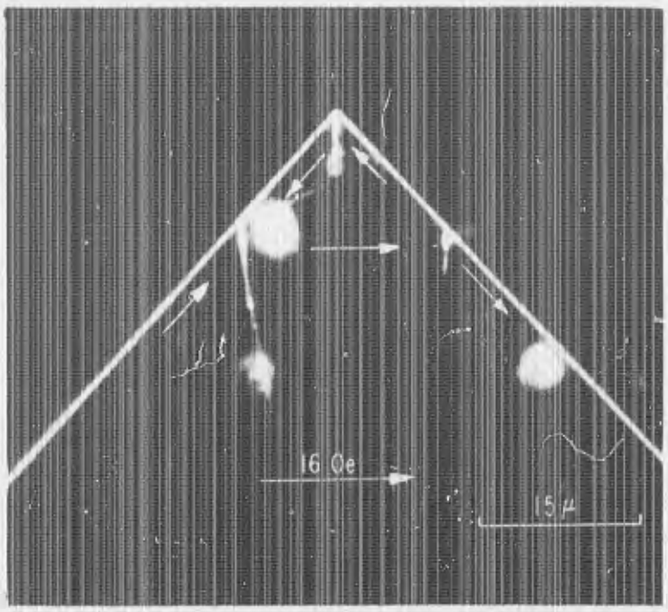


Fig. 36 Nucleus of reverse magnetization at the corner of a Ni-Fe platelet in a diagonal field of 16 Oe. Saturation occurred visibly at an increased field of 65 Oe.

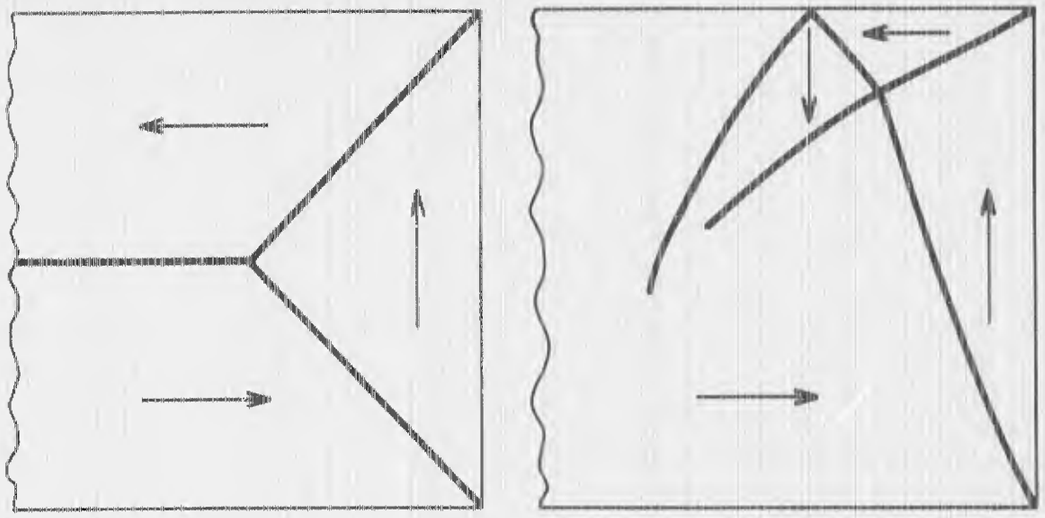

(a) (b)

Fig. 37 (a) Closure pattern at the end of a Ni-Co ribbon in zero field. (b) End pattern after parting of central 180° wall in a field to the right. The flipping of this pattern after application and reduction of a high field indicates saturation.

then in a reduced field a flipped pattern will form, with the magnetization in the domain at the right edge pointing downward. This procedure has been checked with several platelets to see that it works. For example, a 14 μm wide Ni-Co ribbon several thousand angstroms thick required a rotation from alignment of about 2° at 940 Oe for pattern flipping. But adequate quantitative data are still to be obtained. The geometry of Fig. 37, with the field applied parallel to the sides, is of special interest in nucleation theory because of the calculated existence of "infinite" demagnetizing fields at the corners,[61] though Aharoni has shown that this is not a very bothersome "infinity" even for an atomically perfect end.[53]

The observation of saturation at a corner where "infinite" demagnetizing fields exist is closely related to a question that Aharoni posed in his review article on nucleation,[53] namely, whether the negative nucleation fields observed in iron whiskers[62] were less in magnitude than the ideal -560 Oe because saturation in the other direction had not been complete or because imperfections make nucleation intrinsically easier. This question was answered several years ago in favor of easier nucleation in some unpublished work involving the use of miniature, high pulsed field coils.[63] A long iron whisker, 5 μm in diameter, was first tested conventionally[62] with a setting field of 32 Oe and was found to have negative nucleation fields from about 100 to 385 Oe in various regions. No changes in nucleation fields were observed when a surrounding miniature coil applied a setting field of 160 kOe and triggered the conventional test about 200 μsec later, after the critically damped high field pulse was over. Since this field would certainly have brought the region under test to complete saturation and since the nucleation fields did not become more negative, then the nuclei must have been effectively or actually driven out by the 32 Oe setting field and have been regenerated at or near the observed negative nucleation fields. (The qualifications refer to the possibility that a nucleus may form at one field, but not be able to expand and break away from the imperfection where it formed until the field becomes appreciably more negative. Such behavior can, in fact, be observed in submicron nickel whiskers by use of the Bitter technique. A nucleus attached to a sharp cornered end of an $\approx 1/2$ μm diameter whisker may be observed to stretch like a spring in small negative applied fields before breaking away to reverse the magnetization in the whisker at $\approx -25$ Oe.)

Figure 38 contains some qualitative information on nucleation at the edge of a platelet, and also on the effect of the edge nuclei in reducing the magnetostatic energy. In Fig. 38(a) a field of 30 Oe is acting along a ⟨110⟩ easy direction, at 45° with a ⟨100⟩ edge of a nickel platelet. The field had been reduced from 60 Oe, where no nuclei were visible at the edge. A number are now visible, where they make small dents in the bright rim of colloid at the edge and small valleys in the clouds of colloid beyond the edge. In Fig. 38(b) the field is further reduced to 12 Oe. The expanded nuclei now produce regions that are clear of colloid at and beyond the edge. Since colloid collects thickly where there are high field gradients from free poles, the cleared regions indicate the reduction in pole strength, and thus in divergence and magnetostatic energy, resulting from the zigzag closure pattern that the nuclei form at the edge. With regard to nucleation, the spikes did not form at the same positions along the edge with repeated cycling to saturation. This suggests that the edge is so nearly perfect that homogeneous nucleation occurs.

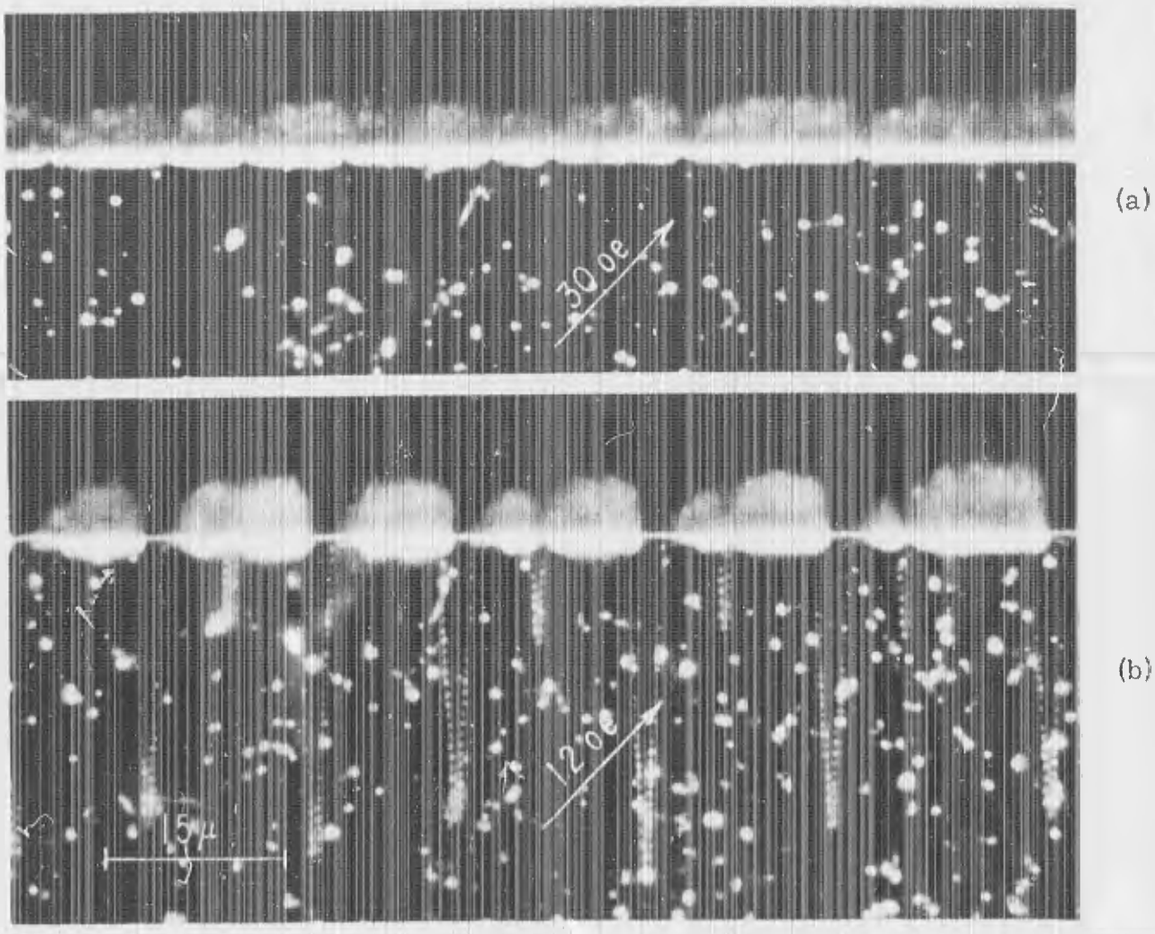


Fig. 38 (a) Colloid pattern at the edge of a nickel platelet in a ⟨110⟩ reduced field of 30 Oe. Several nuclei appear along the edge. (b) Pattern at a reduced field of 12 Oe, showing the growth of the nucleation spikes and the colloid-free regions at their tips.

BLANK PAGE

## VI. MAGNETIZATION REVERSAL IN SUBMICRON WHISKERS

### A. Introduction

In platelets, we have seen that the magnetization is generally subdivided into uniformly magnetized regions, or domains, that form a closure-domain pattern which reduces the magnetostatic energy (external field) to a minimum. The domain walls separating the domains have both finite thickness ($\approx$1000 Å) and energy ($\approx$ 1 erg/cm$^2$), because of anisotropy and exchange energies. [F. Bloch first demonstrated theoretically in 1932 that the region between domains has finite extent.[5] Shortly thereafter, Landau and Lifshitz developed a more precise form for the structure now called a Bloch wall.[6]] In extremely small specimens, on the order of 1000 Å in diameter, the energy of domain walls between closure domains may be greater than the magnetostatic energy that would exist without any domain walls, since these are terms proportional to surface area and volume, respectively, and the latter term decreases more rapidly with decreasing diameter. Thus, at some small size it becomes energetically favorable for a specimen to become a single domain particle. Frenkel and Dorfman had first predicted the existence of such particles in 1930, though their derivation involved a concept not closely germane to domain theory.[64] Kittel[65] made the first pertinent calculations on single domain particles in 1946, and many articles on the subject have followed. [See, for example, the papers by Stoner and Wohlfarth,[66] Luborsky and Morelock,[67, 68] and the review article by Aharoni.[69]]

A major reason for the interest in single domain particles is that they must reverse their magnetization in some other manner than by domain wall motion and thus may require fields for reversal that are several orders of magnitude larger than for the same material in bulk form, e.g., from $10^2$ to $10^4$ Oe instead of $10^{-2}$ Oe. A special case of interest is that of the infinite cylinder.[70-73] Its usual mode of reversal is calculated to be a process called "curling," in which the magnetization has a cylindrically symmetric transverse circumferential component as it deviates from axial alignment in a reverse field.[71-73] The nucleation field, $H_N$, for reversal is[69]

$$-H_N = \frac{2K_1}{M_s} + \frac{1.08(2\pi)A}{R^2 M_s} \qquad (3)$$

where $K_1$ is the magnetocrystalline anisotropy constant; $M_s$ is the saturation magnetization; A is the exchange constant; and R is the cylinder radius. For a nickel cylinder with a 1000 Å diameter, this yields $H_N$ = -400 Oe if we neglect the anisotropy term and take $A = 0.71 \times 10^{-6}$ erg/cm and $M_s$ = 480 emu.

### B. Testing Techniques--Conventional

Nickel whiskers near 1000 Å in diameter commonly grow along with the platelets in the halide reduction process. Luborsky and Morelock have previously measured the coercive forces of random planar dispersions of iron, iron-cobalt, and cobalt whiskers near this size,[67, 68] and it was a natural extension of their work to measure the nucleation fields of the nickel whiskers. This has been done in collaboration with Luborsky.

Even though a 1000 Å whisker is only about one-sixth of a wavelength of light in diameter, it turns out that one may easily see such a whisker under an ordinary stereomicroscope by Rayleigh scattering.[74, 75] It also turns out not to be difficult to remove an individual whisker from the tray where it grows and to place it on a glass slide for testing, by use of a paper fiber held at the end of sharp-pointed tweezers.

Various techniques may be used for determining the nucleation fields in individual whiskers. Luborsky and Morelock used a torque tester and a 60 cps hysteresis loop tracer for whiskers of large size (2 to 200 μm in diameter). Meiklejohn tested iron whiskers as small as 2000 Å in diameter by removing them from the original substrate, gluing them at one end for observation in an optical microscope, and applying a reversing field along with a small transverse field.[67] A sudden change in bending direction occurs when reversal takes place. In some of the earlier work of this study we stuck the whiskers to very thin layers of grease on a glass slide, applied Bitter solution, placed a cover glass on top, and observed the colloidal distribution at an end. If the applied field is opposite the direction of magnetization, then there may be a collection of colloid along the sides of the whisker near the end. But when nucleation occurs and the magnetization reverses to the field direction, then a "candle flame" of colloid extends out from the tip of the whisker. This technique is useful for determining the nucleation field versus the angle $\psi$ between the field and the whisker axis. Figure 39 shows such a curve for a nickel whisker 1600 Å in diameter as measured in an electron microscope. This technique has the disadvantages that the colloid corrodes the whisker, thus changing the nucleation fields during the time of the observations, and that it measures the nucleation fields at the ends, where the sharp corners make nucleation easier than it would be along an infinite cylinder. (The latter disadvantage would be overcome if the whisker were stuck to the slide with its ends curved to form an integral sign, $\int$, so that the center section always forms a smaller angle with the field than the ends.)

## C. Oil Film Technique

A new technique that has proved to be highly versatile and valuable is the oil film technique. Specifically, a whisker is removed from the tray and placed in a thin layer of oil on a glass slide. This is then placed between the

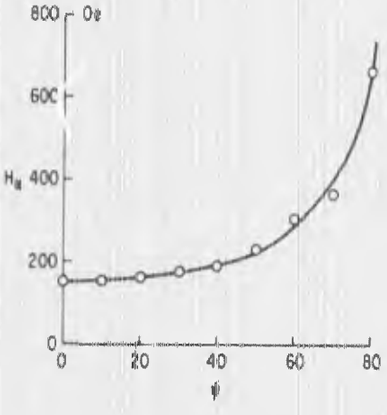


Fig. 39 Plot of nucleation field $H_N$ vs angle $\psi$ between field and whisker axis for a 1600 Å thick nickel whisker.

poles of an electromagnet and the whisker is viewed with a microscope by dark field illumination. A field is applied in one direction to align the whisker, is then reduced to zero, and is gradually increased in the opposite direction. The whisker tends to rotate to the opposite direction, like a compass needle, as long as its magnetization is unreversed. But this tendency is easily countered by properly rotating the microscope stage. When nucleation occurs and reversal of magnetization takes place, the whisker changes to stable equilibrium in the field direction and tends to rotate back through a small angle if the stage is now rotated slightly.

The above technique still yields the nucleation field at an end, rather than for an infinite cylinder, because the sharp corners there act as imperfections. However, if the whisker is thin and long enough and has a high enough nucleation field, then the magnetic forces on the ends of a whisker with its magnetization opposite the field direction suffice to buckle the specimen physically into a curved form such as that shown in Fig. 40(a). This is a photomicrograph of a single-domain nickel whisker (R41), 1070 Å in diameter in a field of 360 Oe. Note that the magnetization is only opposed to the applied field in the upper, central section of the whisker. Nucleation will, therefore, not occur at the ends, but rather at the center, where the magnetization is antiparallel to the field. (This follows both from theory and the experimental observations of Fig. 39.) Thus one may observe nucleation in a nearly perfect specimen under geometric conditions that correspond very closely to the case most thoroughly analyzed theoretically, that of an infinite cylinder.

In an increased field of 395 Oe the ends of the whisker came together and stuck, as shown in Fig. 40(b). The poleless specimen is now almost completely

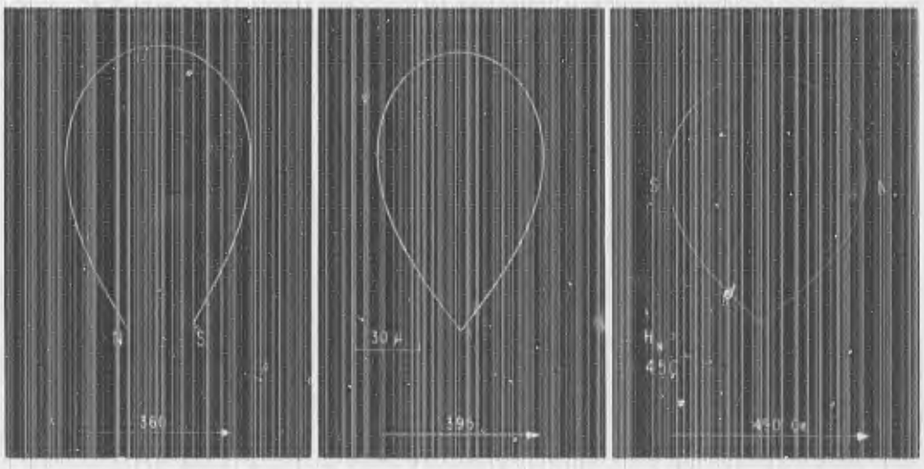


(a) (b) (c)

Fig. 40 (a) Dark-field photomicrograph of a 1000 Å thick single-domain nickel whisker lying in a thin layer of oil and bent into a form of the elastica in a field of 360 Oe. (b) Same whisker in increased field of 395 Oe, with ends stuck together by polar forces. (c) Same whisker at 490 Oe. Nucleation occurred at 450 Oe, resulting in the formation of poles at the left and right regions.

unresponsive to the external field; there was only a barely detectable change in shape in the field range from zero up to the nucleation field. At 450 Oe nucleation occurred at the top center, poles quickly swept to the left and right, and the magnetic forces jerked the specimen to the shape shown in Fig. 40(c).

Figure 41 shows the form a whisker assumes if the ends do not meet and stick together. This is a photomicrograph of another nickel whisker (R45) about 1000 Å in diameter in a 500 Oe field. Nucleation occurred at 515 Oe, again presumably at the top center.

After nucleation, it is easy to maneuver the specimen into the position and form shown in Fig. 42. Here, whisker R41 of Fig. 40 is in a field of 915 Oe and has a north pole at each end and a double-strength south pole at the center. Thus we have created a double-domain "single-domain particle." Symmetry considerations suggest that the magnetization at zero field in the domain wall at the south pole is circumferential at the center and gradually curls, with mirror symmetry, to the opposing axial directions. Thus, there is a zero-dimensional singularity in the spin structure at zero radius at the center of the wall. After a suggestion by C. P. Bean, this might be called a Bloch spot, in conformity with the two-dimensional Bloch wall and the one-dimensional Bloch line. The structure of this Bloch spot would be quite similar to that envisaged by Feldtkeller in the

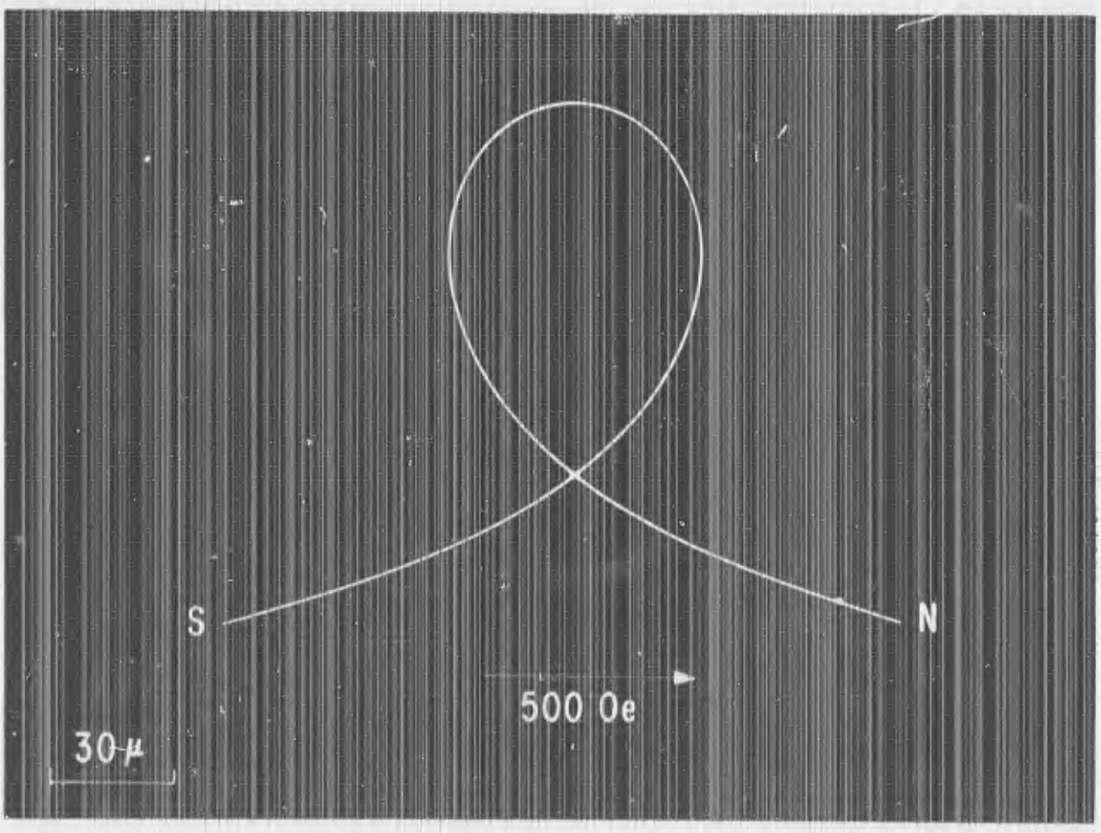


Fig. 41 Photomicrograph of a 1000 Å thick single-domain nickel whisker lying in a thin layer of oil and bent into a form of the elastica in a field of 500 Oe.

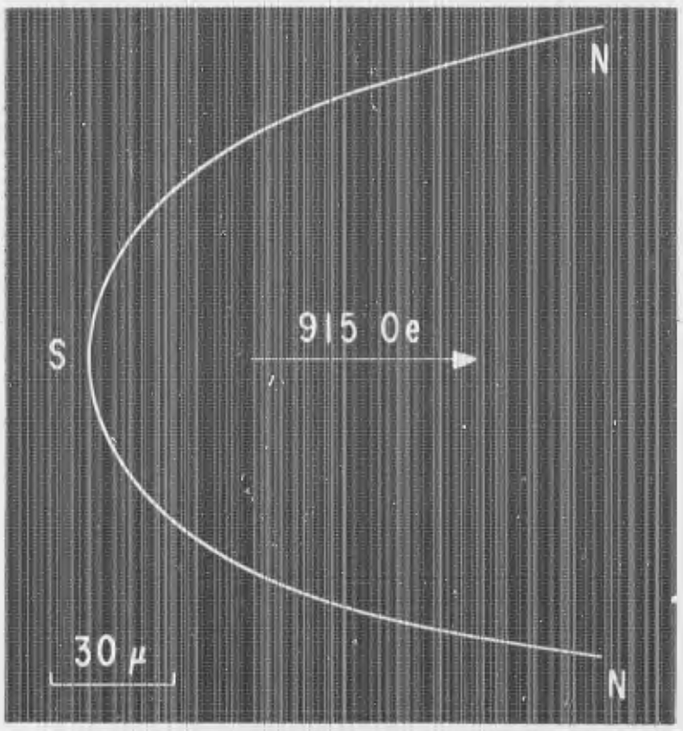


Fig. 42 Whisker of Fig. 40 after nucleation and separation of ends, in a field of 915 Oe. The "single-domain" particle now has two domains, two north poles, and a double-strength south pole.

second of Refs. 24. It is a simple matter to measure the field to sweep the wall itself out of the whisker, or to move it past obstructions, such as a bend or an attached nickel crystallite. In an apparently perfect whisker it requires on the order of 1 Oe to sweep out the pole, but over 100 Oe may be needed to move it past an obstruction.

D. Forms of the Elastica

The shapes that the whiskers have assumed in the above figures are of classical interest in elasticity theory.[76, 77] They are known as "forms of the elastica." The Swiss mathematician, Euler, first derived their differential equation and classified the various forms in 1744. Since one of the terms in the equation is the thickness, the shapes the whiskers assume in a magnetic field provide a means for determining their diameters. However, it is not convenient to analyze the shapes as forms of the elastica, but rather to view sections of the whiskers either as cantilever beams with large deflections,[78] or as circular arcs under pure bending.[79] One may see in Figs. 40(a), 41, and 42 that the sections of the whiskers from the ends to where they are tangent to a vertical line represent highly deflected cantilever beams. One may also see that the center sections of Figs. 40(a) and 41 have nearly constant radii of curvature for approximately ±40°. This is so because the long lever arms from the poles to the center sections leave these regions under almost pure bending moment. From elasticity theory it is easy to show that the bending thickness, D, is

$$D \approx \left(\frac{12\ \rho \ell\, H M_s}{E}\right)^{1/2} , \qquad (4)$$

where $\rho$ is the radius of curvature; $\ell$ is the lever arm; H is the applied field; $M_S$ is the saturation magnetization; and E is Young's modulus.

If the whisker is rectangular, it will bend about the smaller thickness. Furthermore, the larger thickness cancels out in the derivation of Eq. (4). However, both dimensions of a rectangular whisker are important in nucleation theory. Also, one may not simply use a handbook value for Young's modulus in Eq. (4). There is a qualitatively well known dependence of this modulus on magnetic state, the "$\Delta E$" effect. Therefore, the experimental procedure has been to obtain the nucleation and bending data first. Then the whisker is transferred to the grid of an electron microscope, where its thickness and crystallographic orientations are determined. Because the whiskers are quite small, not all the attempted transferrals and orientation determinations were successful. Figure 43 is a photomicrograph of a nickel whisker, R59, 73 μm long and 590 Å thick, mounted on a grid. Only 22 μm of its length shows up, beyond the globule. The rest is sticking to the side of a thicker nickel whisker that was used to transfer it from the oil to the grid. The mass of the whisker is impressively small, $2.3 \times 10^{-12}$ gram, or 2.3 pg.

E. Nucleation Field vs Thickness

Table I shows thickness, orientation, nucleation, and bending data for a number of whiskers. The first eight (R33 through R61b) were positioned in the

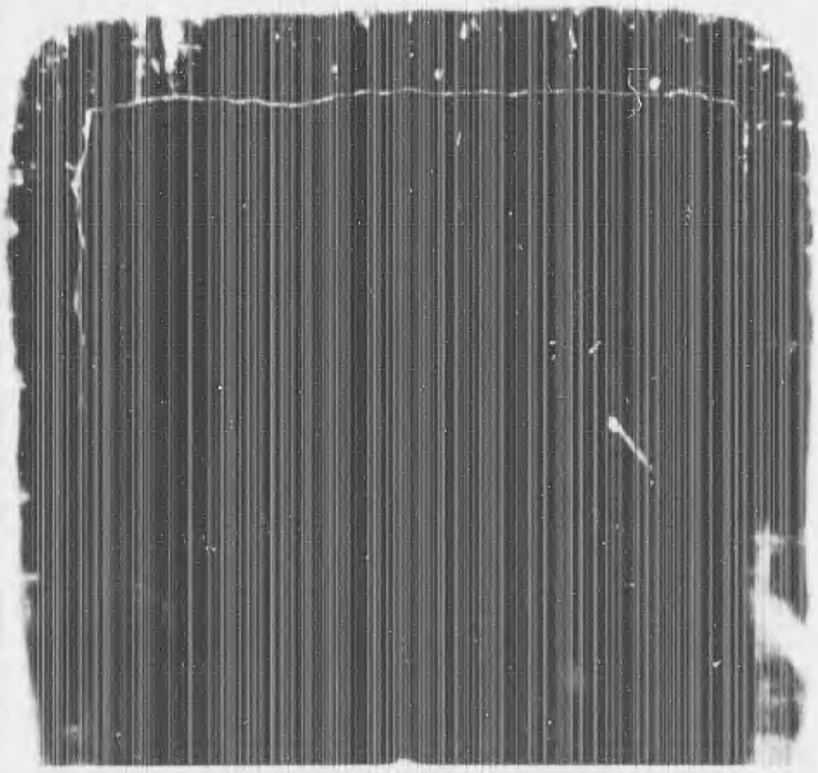

Fig. 43 Photomicrograph of a 590 Å thick nickel whisker mounted on an electron microscope grid.

TABLE I

Nucleation, thickness, crystallographic, and bending data for 23 submicron nickel whiskers. E.M. D(Å) is the whisker thickness (in angstroms) observed in an electron microscope, and the next two columns show the plane perpendicular to the electron beam and the whisker axis index as determined by electron diffraction. Calc. D(Å) is the calculated thickness (where needed or available) of the assumedly square whisker. $H_Y$ is the nucleation field $H_N$ at the center of a whisker elastically bent into a form of the elastica; $H_{e1}$ and $H_{e2}$ are the nucleation fields at the whisker ends; ρ is the radius of curvature at the center of the whisker elastically bent into a form of the elastica in a field H(Oe); ℓ is the lever arm from a whisker tip to the center of the whisker with radius of curvature ρ and in field H; E is Young's modulus as calculated from the bending data; and D/2ρ is the central bending strain for the corresponding values of ρ, H, and ℓ.

| No. | E.M. D(Å) | {hjk} | ⟨hjk⟩ | Calc. D(Å) | $H_N$(Oe) $H_Y$ | $H_e$ | $H_{e2}$ | ρ(μm) | H(Oe) | ℓ(μm) | E(dyn/cm²) | $\frac{D}{2\rho}$ |
|---|---|---|---|---|---|---|---|---|---|---|---|---|
| R33 ○ | 1160 | 100 | 100 | | 390 | 270 | 265 | | | | | |
| R35 ○ | 800 | 100 | 100 | | 840 | 590 | 500 | 17.9 | 790 | 65.7 | $8.4 \times 10^{11}$ | $2.23 \times 10^{-3}$ |
| R37 ○ | 1170 | 100 | 100 | | 460 | 315 | 310 | 38.0 | 447 | 107.5 | 7.5 | 1.54 |
| R40 ○ | 720 | 100 | 100 | | 780 | 700 | 590 | 35.4 | 720 | 35.4 | 10.1 | 1.02 |
| R41 ○ | 1070 | 100 | 100 | | 455 | 325 | 315 | 36.9 | 420 | 123.0 | 9.6 | 1.45 |
| R50 ○ | 1070 | 100 | 100 | | 395 | 315 | 255 | 46.2 | 300 | 156.0 | 11.0 | 1.16 |
| R59 ○ | 590 | 100 | 100 | | 1020 | 930 | 830 | | | | | |
| R61b ○ | 1140 | 100 | 100 | | | 320 | 285 | | | | | |
| R61a △ | 1530 | 110 | 100 | 1025 | 325 | 310 | 255 | 55.9 | 208 | 210.5 | 13.5 | 0.92 |
| R51 △ | 975 | 110 | 100 | 690 | 660 | 635 | 490 | 38.2 | 208 | 174.3 | 16.9 | 0.90 |
| R52 △ | 905 | 110 | 100 | 640 | 730 | 715 | 535 | 18.8 | 700 | 61.6 | 11.5 | 1.70 |
| R58 △ | 625 | 110(?) | 100 | 440(?) | 1180 | 1220 | 1210 | 14.1 | 890 | 52.4 | 19.7 | 1.56 |
| R30 × | 2760 | 111 | 110 | 1980 | | | 190 | | | | | |
| R36 □ | 945 | | 100 | | | | 405 | | | | | |
| R38 ▽ | 800 | | | | 1420 | 1290 | | | | | | |
| R39 ▽ | 1010 | | | | 540 | 460 | 400 | | | | | |
| R42 ∠ | 825 | $1\bar{2}0$ | 100 | 760 | 765 | 800 | 660 | | | | | |
| R43 + | 1010 | 110 | 110 | | 670 | 510 | 440 | | | | | |
| R44 ▽ | 620 | | 100 | | 910 | 700 | 615 | | | | | |
| R49 □ | 690 | | | | | 595 | 575 | | | | | |
| R53 ▽ | 850 | | 100 | | 650 | 560 | 540 | | | | | |
| R55 ▽ | 770 | | 100 | | 710 | 720 | 695 | | | | | |
| R56 ▽ | 855 | | | | 700 | 720 | | | | | | |

electron microscope to give {100} ⟨100⟩ electron diffraction patterns. (The specimen can be rotated in the apparatus by about ±12°.) Since specimens with ⟨100⟩ axial orientation have {100} sides (this being known from previous experience with whisker growing), the thicknesses measured by the electron microscope are correct if the whisker is square. However, there might be a tendency for a rectangular whisker to lie on its broader side. On the other hand, the selection process of finding whiskers with high nucleation fields and sweeping away the others would tend to favor those that are nearly square. In any case, these thicknesses have been used in Eq. (4) to calculate the effective value for Young's modulus. For each whisker one or more photographs were analyzed for radius of curvature ρ and lever arm ℓ for given field H. The handbook value for E is $21 \times 10^{11}$ dyn-cm$^{-2}$. Curves of the ΔE effect in bulk specimens show reductions to as low as $18 \times 10^{11}$ dyn-cm$^{-2}$ at room temperature. Thus the ΔE effect appears to be much greater for the whiskers. The question of how rectangular the whiskers are is still of concern, since Young's modulus varies inversely as the square of the thickness. One imaginable experimental procedure for the future

would be to anchor one end, bring the whisker into resonance in air or vacuum for vibration about each thickness, and determine the thickness ratios from the resonance frequency ratios, after the procedure of Murphy and Sears.[80] The $\Delta E$ effect could be calculated for whiskers from Brown's[23, 81] or Tiersten's[82] independently derived theories involving magnetostriction, but the calculations, while important for elasticity theory, would be extremely tedious.

In Table I, $H_\gamma$ is the nucleation field for the central section of the whisker, corresponding closely to that for an infinite cylinder, while $H_{\epsilon 1}$ and $H_{\epsilon 2}$ are the end nucleation fields. The latter are obtained, one at a time, by rotating the stage rather rapidly so as to maintain one end of the whisker with its magnetization antiparallel to the applied field. Nucleation leads to a sudden decrease in the radius of curvature at the center and, of course, to a cessation of the whisker's rapid rotation.

Whiskers R61a through R58 showed {110} ⟨100⟩ orientations. These whiskers probably have {100} sides, so that the electron beam passed perpendicular to an approximately diagonal {110} plane. Thus, if the whisker is a square, the true thickness is $D/\sqrt{2}$. The calculated thicknesses of whiskers R51, R52, and R58 were found this way. However, whisker R61 was a long one that broke in two with handling. Data on both sections were obtained in the electron microscope. Direct geometric calculations give the smaller thickness as 1025 Å and a Young's modulus of $13.5 \times 10^{11}$ dyn-cm$^{-2}$. Since the $\Delta E$ effect may depend on the strain, this is given in the last column for the analyzed photographs. Whiskers R51 and R58 have relatively high values of E, but both whiskers were bent, so that the results are suspect.

The thicknesses of whiskers R30 through R56 were measured, but the orientation data are either odd or incomplete. Among the whiskers lost in transfer and not recorded in Table I are R46, R47, and R60, with $H_\gamma$ of 1560, 1120, and 1270 Oe, respectively. If further experiments show a useful average value for Young's modulus, then the approximate thicknesses of these whiskers may be determined from the available bending data. More data remain to be analyzed. A journal article to be written in collaboration with F. E. Luborsky is planned for the near future and should contain additional results and more extensive conclusions than are included in this section.

Figure 44 is a log-log plot of nucleation field (absolute value) vs thickness. The symbols correspond to those listed with each whisker in Table I. Nucleation field $H_\gamma$ is plotted when available (o, Δ, ▽, +); otherwise, an end nucleation field, $H_\epsilon$, is plotted (□, x). The uncorrected electron microscope thickness is plotted for symbols □ and ▽. On the lower right region of the graph are nine data points (□) not included in the table since they did not bend and no electron diffraction data were taken on them.

The solid diagonal line of Fig. 44 is the theoretical curve for curling in an infinite circular cylinder [the second term of Eq. (3)]. The dashed lines are the theoretical upper and lower limits for curling in an infinite square cylinder with side D.[69] The calculations assume $M_s = 480$ emu and $A = 0.71 \times 10^{-6}$ erg/cm. The latter constant is not accurately known. Thus the correct positions for the lines might be appreciably shifted from those shown. Nevertheless, the data below about 1200 Å match the shown theoretical predictions for curling

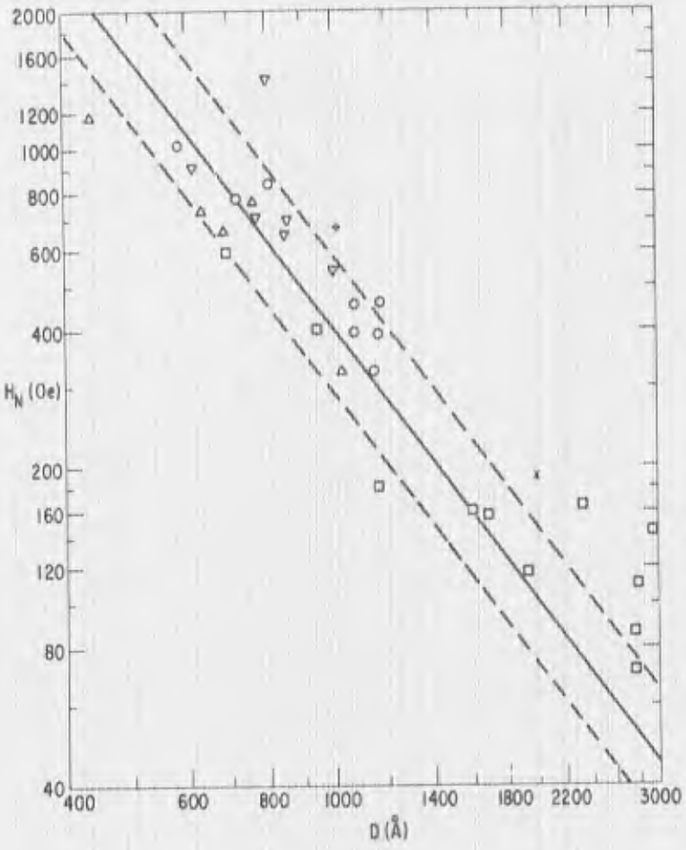


Fig. 44 Plot of nucleation field $H_N$ vs thickness D from the nickel whisker data of Table I. The different symbols match different sets of data, as shown in Table I. The solid line is that calculated theoretically for curling in an infinite circular cylinder of nickel with diameter D. The dashed lines are the upper and lower theoretical limits for a square infinite cylinder of nickel with side D.

fairly closely. The high position of data point R43 (+) may result from magnetocrystalline anisotropy [the first term of Eq. (3)] since ⟨110⟩ are almost directions of minimum anisotropy and the first term can add as much as 180 Oe to the magnitude of the nucleation field for nickel at room temperature. The high position of data point R38 (▽) might mean that the correct thickness is about 800/$\sqrt{2}$ Å. The diffraction spots for whisker R58 were of such poor quality that the assignment {110} was originally recorded only as a reasonable guess. The plane might actually be {100}, in which case the uncorrected thickness of 625 Å would be used and would better match the other data.

F. Nucleation Field vs $\psi$

We have seen from Fig. 39 that the nucleation field $H_N$ increases with increasing angle $\psi$ between the field and the whisker axis. But the Bitter technique used to obtain these data was not satisfactorily precise because of corrosion. Luckily, whisker R45 fragmented into several segments after lying in an oil film for about 2 months. Figure 45 is a double exposure of one of these

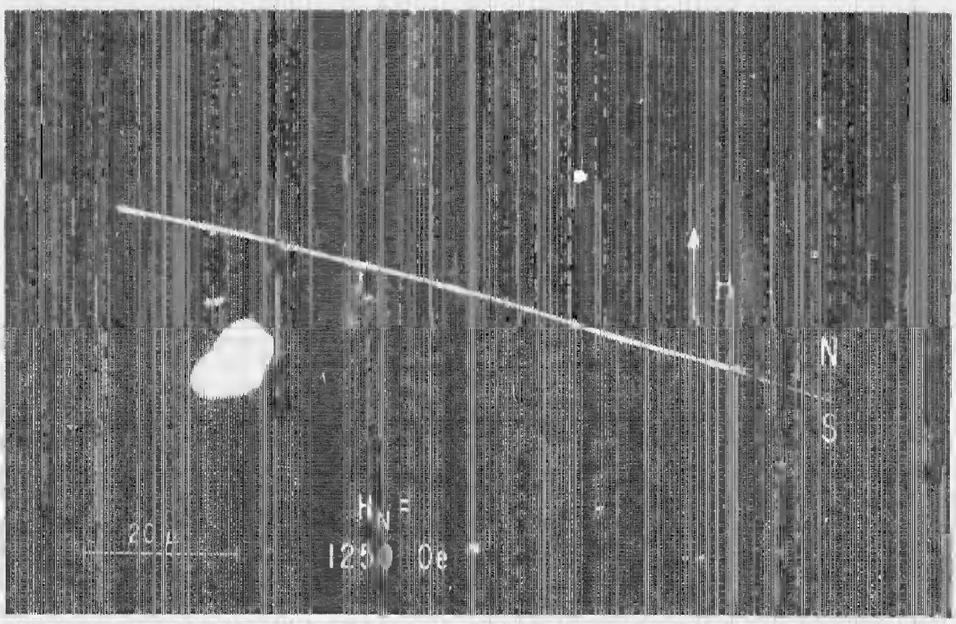


Fig. 45 Double-exposure photomicrograph of a segment of the whisker of Fig. 41 after fracture. Only the right end is free to move. It serves as an indicator of nucleation, being deflected upward before nucleation and downward after nucleation.

segments. It is stuck in position except for the right end. The first exposure was taken when the applied field was slightly less than the nucleation field of 1250 Oe for the shown field-whisker orientation, and the unreversed north pole to the right is deflected upward. When nucleation occurred, the right end became a south pole and suddenly flicked down to the position shown. Thus the right end serves as a nucleation indicator. Since both ends form larger angles with the field than does an internal region near the right end, the observed nucleation field is probably nearly that of an infinite cylinder. The data points of Fig. 46 show the nucleation field $H_N$ (right-hand ordinate) vs angle $\psi$ for this whisker segment for a sequence of data taken at high values of $\psi$. The $\psi = 0$ nucleation field of 570 Oe indicates that the thickness of the whisker is about 950 Å.

The solid curve labeled "curling" is one of a set of theoretical curves calculated by Shtrikman and Treves.[83] It shows the reduced nucleation field $h_n$ (left-hand ordinate) vs angle $\psi$ for a circular cylinder with reduced diameter $S = 2.2$, corresponding to an approximate diameter of 770 Å for a nickel cylinder. [$S \equiv D/D_0$, where reversal occurs by coherent rotation rather than by curling for $D \ll D_0$. $h_n \equiv H_N/H_0$, where $H_0$ is the nucleation field for coherent rotation at $\psi = 0$.[66, 71]] The dashed curve labeled "coherent" was calculated by Stoner and Wohlfarth[66] for the reversal mode in which all spins remain parallel to each other during the process. Shtrikman and Treves predicted that where the

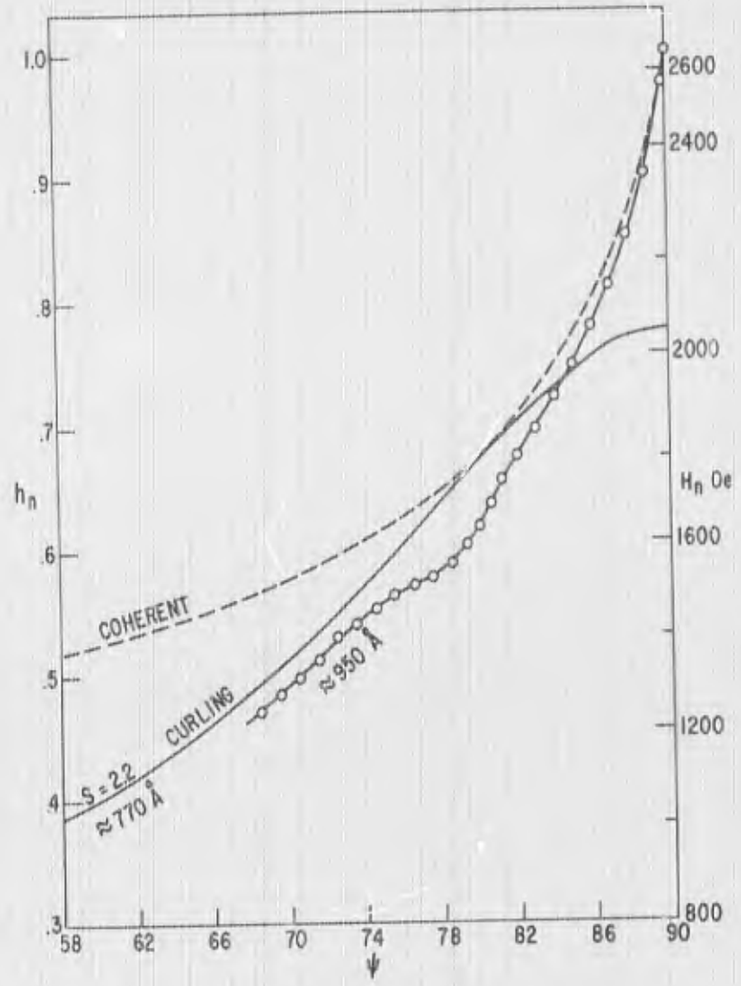


Fig. 46 Plot of nucleation field $H_N$ (right ordinate) vs angle $\psi$ between field and whisker axis for the nickel whisker segment of Fig. 45. The solid line labeled "curling" is a theoretical curve of reduced nucleation field $h_n$ (left ordinate) vs $\psi$. The dashed line labeled "coherent" is a similar theoretical curve for reversal by coherent rotation. The experimental curve changes from the curling mode to the coherent mode of reversal where the theoretical curves meet.

"curling" and "coherent" curves meet, the magnetization reversal mode would pass over to the coherent mode at larger $\psi$ because the lower energy curling mode cannot be reached without passing through the coherent mode.[83, 67] The experimental curve of Fig. 46 is for a square or rectangular cylinder rather than for a circular cylinder, and the reduced diameter is greater than 2.2, but the curve does clearly follow the coherent mode at angles above 80°, and the dip in the curve near 78° probably corresponds to the crossover.

C. Invisible Segments

Other segments of whisker R45 of Fig. 45 showed a surprising behavior that might be of interest to those studying light scattering. Figure 47(a) shows several segments with apparent gaps in between. However, in an applied field

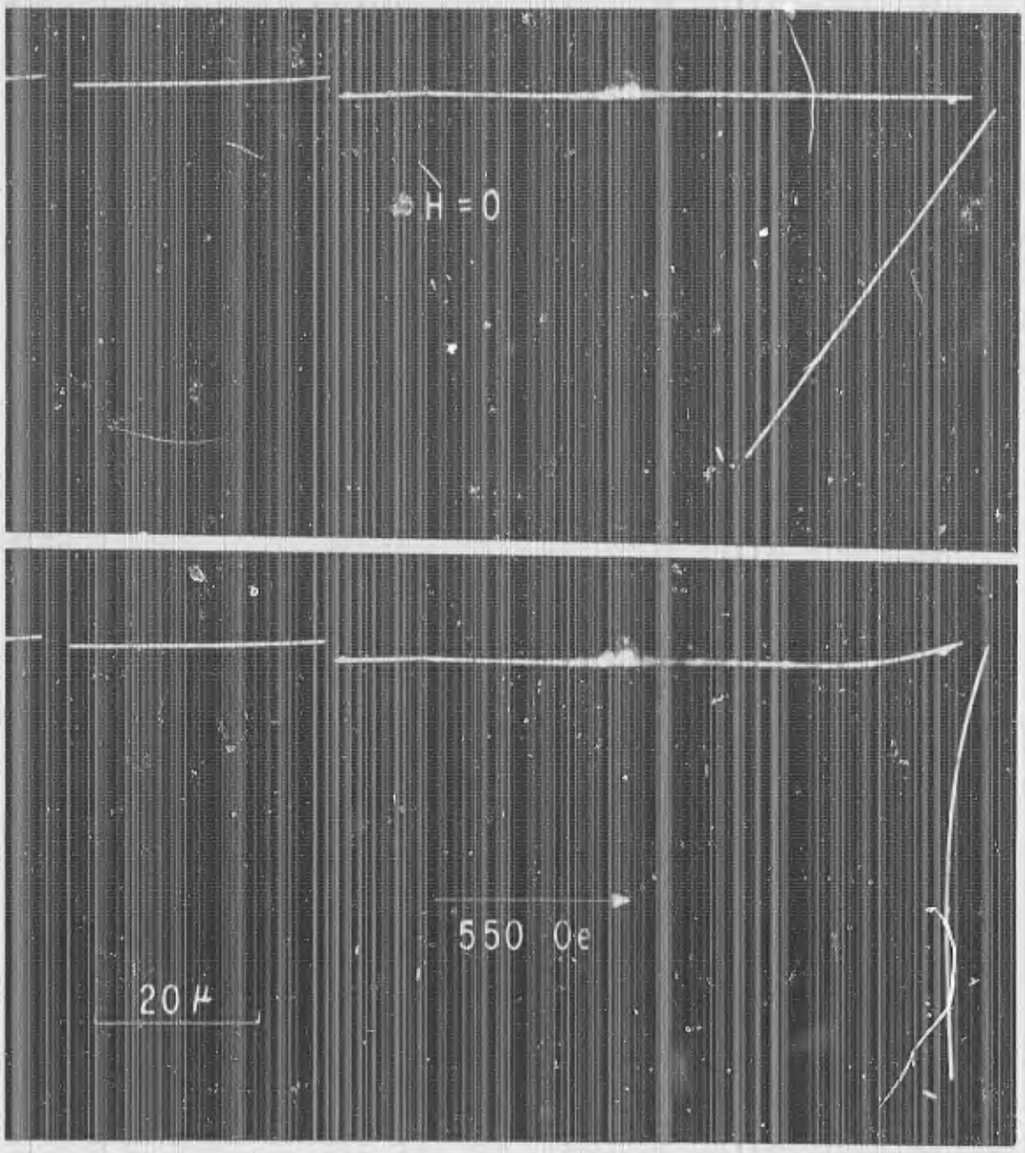


Fig. 47 (a) Further segments of the whisker of Fig. 41 after fracture. They appear not to be joined. (b) The bending and rotation of the right-hand segments in a field of 550 Oe demonstrate that material does still join the segments.

the right-hand segments bent and rotated in a manner that shows they are connected [Fig. 47(b)]. The invisible connecting segments are probably ribbons that formed when the whisker sheared along crystallographic glide planes, much as one might picture shearing in a stack of adhering cards. But if one dimension, probably the vertical one, is still about the same as that of the whisker, then why is the dark field illumination not visibly scattered?

## VII. MISCELLANY

### A. Platelet Growth

The platelets have all been grown from commercial grade chemicals (the -ous bromides of nickel, cobalt, and iron from Amend Drug and Chemical Co., Inc., New York, and British Drug Houses Ltd., Poole, England). Several attempts to grow nickel platelets from 99.9% pure material (Gallard-Schlesinger Chemical Mfg. Corp., Carle Place, New York) were not successful. This shows the apparent need for impurities to nucleate the growth of the platelets.[2]

A recent attempt to grow Ni-Fe platelets of the Permalloy composition used for thin-film memory elements (81% Ni) was successful. Previous attempts had resulted in thick platelets with small percentages of iron. The success may be due to the fact that the Vycor tube cracked in the furnace during the growth period. This may, for example, have allowed some oxygen to diffuse in. This clue will be followed up. The growth started with 20 grams $FeBr_2$ and 10 grams $NiBr_2$ (both hydrous). The gas flow was about 100 $cm^3$/min (0.2 S.C.F.H.) of nitrogen and about ten 1-mm-diameter bubbles of hydrogen per second ($\approx$0.3 $cm^3$/min). The furnace was heated to 800°C in about a half hour and was kept there overnight.

Thin platelets of pure iron may be grown by a vapor transport method.[7,15,84] This method has not yet been tried here, but it might prove to be of interest in the future.

### B. Platelet Mounting

One item of the contract has been to supply platelets to the Microwave Physics Laboratory as needed for in-house research. A square nickel platelet about 1500 Å thick and one-third millimeter on a side was recently mounted on an optically flat quartz rod for M. H. Seavey for a magneto-acoustic experiment. Platelets of this thickness adhere firmly to any flat surface without any bonding material. The distance between quartz and platelet is probably less than a couple hundred angstroms except at several small regions where air or small particles are entrapped. No light interference fringes were visible when the under surface of the platelet was viewed through the quartz rod. Thinner platelets ($\lesssim$1000 Å) are difficult to mount satisfactorily because they generally wrinkle excessively as they draw themselves to the mounting surface. Thicker platelets ($\gtrsim$2500 Å) are difficult to mount in such close contact because any particle between the surfaces will wedge up the whole platelet, i.e., it is too thick to cup down over the particle. This problem could be overcome with hyperclean surfaces.

### C. Ferromagnetic Resonance

D. S. Rodbell has used the nickel platelet for ferromagnetic resonance studies and has obtained very narrow resonance line widths (which indicate a high degree of perfection) and from which he could extract an "intrinsic damping" parameter, $\lambda = 2.5 \times 10^8$ $sec^{-1}$.[14] Attempts to grow purer platelets were

aimed at seeing if this parameter could be reduced in value. However, more recent resonance experiments with Ni-Co platelets have also yielded similarly narrow line widths.[85] This suggests that the substitution of a small uniform percentage of cobalt atoms for nickel atoms in a structurally perfect crystal lattice has little effect on the damping process. [Some wide resonance lines that Z. Frait measured earlier for some Ni-Co platelets grown at this laboratory may have resulted from nonuniform composition such as that shown by the platelet of Fig. 10.[86]] There is still a question of the influence of interstitial hydrogen on the resonance line width, and also on the "aftereffect" observed in thin platelets.[2] It is planned to vacuum anneal some platelets to remove the hydrogen and see if this has an effect on either experiment.

D. Pentagons

It is well known that a periodic crystal lattice cannot have fivefold rotational symmetry. In 1959, Melmed and Hayward observed submicron whiskers of nickel, iron, and platinum with fivefold symmetry among those grown for field emission studies.[87] Since then, a number of structures with apparent fivefold symmetry have been observed. The most recent report by Downs and Braun[88] contains references to most of the previous observations, including the pentagonal whiskers that are commonly found in large numbers among the growths of nickel platelets. The crystal structure may be described as having a ⟨110⟩ axis, {100} sides, and {111} twin planes at each corner.[1,2,87] There is also either a 7°20' bend in one of the faces to accommodate the difference between a perfect pentagon and one formed by five {111} twin planes, or a distribution of this mismatch in lattice strain or imperfections in the twin planes.

Bagley has pointed out that it is highly unlikely that the whiskers form by a fivefold twinning process.[89] He proposes, rather, that they nucleate and grow as pentagonal structures, and he develops a hard-sphere model showing how this might occur. This proposal does not conflict with the initial statement about a periodic lattice, since the whisker does not form a periodic lattice. His model would allow packing to infinity, but the structure would have a unique axis, the fivefold rotational axis of the initial nucleus. The profuse growths of pentagonal whiskers provide strong support of his proposal. It is probable that the whiskers nucleate and grow initially as perfect pentagons, in accord with the observations of Melmed and Hayward.[87] The 7°20' jog observed on one face of the larger nickel whiskers would then represent a late stage in the growth, when it has grown to such a diameter (perhaps >1 μm) that the strain energy density becomes relatively important and favors further growth of a pseudo-pentagonal form.

E. Motion Picture Showing Nucleation

A 16 mm motion picture showing the physical bending of ≈1000 Å thick nickel whiskers into forms of the elastica, and the nucleation of the reversal of magnetization in these whiskers at high fields, has been taken with the help of photographer Kenneth Hay and has been edited into a four-minute reel. Titles and descriptive material still need to be added. When this is done, we plan to make copies available as an educational film.

## ACKNOWLEDGMENTS

I wish to thank E. Lifshin for the electron microscope analyses of thickness and composition, and for developing the analytical procedure and computer program that made this possible. I also wish to thank E. Koch for measuring the whisker thicknesses and for taking and analyzing the electron diffraction data. The whisker nucleation study is being carried out in collaboration with F. E. Luborsky. Helpful discussions with D. S. Rodbell and C. P. Bean are also acknowledged.

## REFERENCES

1. R.W. DeBlois, J. Appl. Phys., 36, 1647 (1965).
2. R.W. DeBlois, J. Vac. Sci. Technol., 3, 146 (1966).
3. R.W. DeBlois, J. Appl. Phys. (to be published March 1967, abstract only).
4. P. Weiss, J. Phys., [4] 6, 661 (1907).
5. F. Bloch, Z. Physik, 74, 295 (1932).
6. L. Landau and E. Lifshitz, Physik. Z. Sowjet., 8, 153 (1935).
7. R. Gemperle, Phys. Stat. Sol., 14, 121 (1966).
8. S. Chikazumi, Physics of Magnetism, John Wiley and Sons, Inc., New York (1964), p. 119.
9. C. Kittel, Phys. Rev., 110, 1295 (1958).
10. M.H. Seavey, Jr. and P.E. Tannenwald, Phys. Rev. Letters, 1, 168 (1958).
11. Z. Frait and B. Heinrich, J. Appl. Phys., 35, 904 (1964).
12. P.E. Wigen, W.I. Dobrov, and M.R. Shanabarger, Phys. Rev., 140, A1827 (1965).
13. M. Nisenoff and R.W. Terhune, J. Appl. Phys., 36, 732 (1965).
14. D.S. Rodbell, Phys., 1, 279 (1965).
15. Z. Frait, D. Fraitová, M. Kotrbová, and Z. Hauptman, Czech. J. Phys., B16, 837 (1966).
16. S. Middelhoek, Ferromagnetic Domains in Thin Ni-Fe Films, Drukkerij Wed. G. van Soest N.V., Amsterdam (1961), p. 37.
17. D.H. Martin, Proc. Phys. Soc. (London), B70, 77 (1957); D.H. Martin and D. Bloor, 73, 695 (1959).
18. L. Néel, J. Phys. Radium, 5, 241 (1944); Cahiers phys., 25, 21 (1944).
19. H.J. Williams, R. Bozorth, and W. Shockley, Phys. Rev., 75, 155 (1949).

20. L.F. Bates and F.E. Neale, Proc. Phys. Soc. (London), A63, 374 (1950); L.F. Bates and C.D. Mee, A65, 129 (1952); L.F. Bates and A. Hart, B69, 497, 1200 (1956); L.F. Bates, 84, 625 (1964).

21. E.W. Lee, Proc. Phys. Soc. (London), A66, 623 (1953).

22. W.F. Brown, Jr., Magnetostatic Principles in Ferromagnetism, North-Holland Publishing Co., Amsterdam (1962), p. 121.

23. W.F. Brown, Jr., Magnetoelastic Interactions, Springer-Verlag, Inc., New York (1967).

24. E. Feldtkeller, in Basic Problems in Thin Film Physics, R. Niedermayer and H. Meyer, eds., Vandenhoeck and Ruprecht, Göttingen (1966), p. 451; Z. angew. Phys., 17, 121 (1964).

25. S. Middelhoek, J. Appl. Phys., 34, 1054 (1963).

26. S. Middelhoek, J. Appl. Phys., 37, 1276 (1966).

27. E. Feldtkeller, Elektron. Rechenanl., 3, 167 (1961); in Electric and Magnetic Properties of Thin Metallic Layers, Koninklijke Vlaamse Academie voor Wetenschappen, Lettern en Schone Kunsten van Belgie, Brussels (1961), p. 98.

28. R.W. DeBlois, J. Appl. Phys., 36, 1063 (1965) (abstract only).

29. E.J. Török, A.L. Olson, and H.N. Oredson, J. Appl. Phys., 36, 1394 (1965).

30. R.J. Spain, Appl. Phys. Letters, 3, 208 (1963).

31. N. Saito, H. Fujiwara, and Y. Sugita, J. Phys. Soc. Japan, 19, 421 (1964); ibid., 1116.

32. J. Kaczér, M. Zelený, and P. Šuda, Czech. J. Phys., 13, 579 (1963).

33. Y. Sugita and H. Fujiwara, J. Phys. Soc. Japan, 20, 98 (1965).

34. R.J. Spain and H.W. Fuller, J. Appl. Phys., 37, 953 (1966).

35. T. Iwata, R.J. Prosen, and B.E. Gran, ibid., p. 1285.

36. A. Baltz, ibid., p. 1485.

37. Y. Murayama, J. Phys. Soc. Japan, 21, 2253 (1966).

38. A. Bourret and D. Dautreppe, Phys. Stat. Sol., 13, 559 (1966).

39. H.J. Williams and R.C. Sherwood, J. Appl. Phys., 28, 548 (1957).

40. M. Paulus, Compt. Rend., 250, 1213 (1960).

41. M.E. Hale, Fifth National Symposium on Vacuum Technology Transactions, Pergamon Press, New York (1959), p. 215.

42. H.W. Fuller, H. Rubinstein, and D.L. Sullevin, J. Appl. Phys., 32, 286S (1961).

43. E. Feldtkeller and W. Liesk, Z. angew. Phys., 14, 195 (1962).

44. D.O. Smith and K.J. Harte, J. Appl. Phys., 33, 1399 (1962).

45. M.S. Cohen, J. Appl. Phys., 34, 1221 (1963).

46. J. Kaczér, J. Appl. Phys., 29, 569 (1958).

47. R.E. Behringer, ibid., p.1380.

48. R. Collette, J. Appl. Phys., 35, 3294 (1964).

49. W.F. Brown, Jr., and A.E. LaBonte, J. Appl. Phys., 36, 1380 (1965).

50. A.E. LaBonte and W.F. Brown, Jr., J. Appl. Phys., 37, 1299 (1966).

51. A. Aharoni, ibid., p.3271.

52. W.F. Brown, Jr., Rev. Mod. Phys., 17, 15 (1945).

53. A. Aharoni, Rev. Mod. Phys., 34, 227 (1962).

54. C.A. Fowler, Jr., E.M. Fryer, and D. Treves, J. Appl. Phys., 32, 296S (1961).

55. C. Guillaud, J. Phys. Radium, 12, 492 (1951).

56. R.C. Sherwood, J.P. Remeika, and H.J. Williams, J. Appl. Phys., 30, 217 (1959).

57. J.S. Shur, E.W. Shtolz, and W.I. Margolina, Zh. Eksperim. i Teor. Fiz., 38, 46 (1960) [Soviet Phys. - JETP 11, 33 (1960)].

58. H. Kojima and K. Gotō, in Proc. Intern. Conf. on Magnetism, Nottingham, September 1964, Inst. Phys. and Phys. Soc., London (1965), p. 727.

59. J.S. Shur, ibid., p. 776; J.S. Shur, A.A. Glaser, Yu. N. Dragochansky, V.A. Zaikova, and G.S. Kandaurova, Izvest. Akad. Nauk SSSR, 28, 553 (1964).

60. G.S. Kandaurova and Ya. S. Shur, Fiz. Metal. i Metalloved., 20, 673 (1965) [Soviet Phys. - Met. Metallog., 20, 33 (1965)].

61. S. Shtrikman and D. Treves, J. Appl. Phys., 31, 72S (1960).

62. R.W. DeBlois and C.P. Bean, J. Appl. Phys., 30, 225S (1959); R.W. DeBlois, 32, 1561 (1961).

63. R.W. DeBlois, Rev. Sci. Instr., 32, 816 (1961); R.W. DeBlois and D.S. Rodbell, Phys. Rev., 130, 1347 (1963).

64. J. Frenkel and J. Dorfman, Nature, 126, 274 (1930).

65. C. Kittel, Phys. Rev., 70, 965 (1946).

66. E.C. Stoner and E.P. Wohlfarth, Phil. Trans. Roy. Soc. (London), A240, 599 (1948).

67. F.E. Luborsky and C.R. Morelock, J. Appl. Phys., 35, 2055 (1964).

68. F.E. Luborsky and C.R. Morelock, in Proc. Intern. Conf. on Magnetism, Nottingham, September 1964, Inst. Phys. and Phys. Soc., London (1965), p. 763.

69. A. Aharoni, Phys. Stat. Sol., 16, 3 (1966).

70. E. Kondorskii, Izvest. Akad. Nauk SSSR, Ser. Fiz., 16, 398 (1952).

71. E.H. Frei, S. Shtrikman, and D. Treves, Phys. Rev., 106, 446 (1957).

72. W.F. Brown, Jr., Phys. Rev., 105, 1479 (1957); J. Appl. Phys., 30, 62S (1959).

73. S. Shtrikman and D. Treves, in Magnetism, Vol. III, G.T. Rado and H. Suhl, eds., Academic Press, New York (1963), p. 395.

74. Lord Rayleigh, Phil. Mag., 12, 81 (1881).

75. For an entry to current literature, see, for example, A.H. Lind and J.M. Greenberg, J. Appl. Phys., 37, 3195 (1966).

76. A.E.H. Love, A Treatise on the Mathematical Theory of Elasticity, 4th ed., Dover Publications, New York (1944), p. 401.

77. R.P. Feynman, R.B. Leighton, and M. Sands, The Feynman Lectures on Physics, Addison-Wesley Publishing Co., Inc., Reading, Mass. (1964), Chap. 38, p. 12.

78. K.E. Bisshopp and D.C. Drucker, Quart. Appl. Math., 3, 272 (1945).

79. S. Timoshenko and G.E. MacCullough, Elements of Strength of Materials, 2nd ed., D. Van Nostrand Co., New York, (1940), p. 151.

80. W.K. Murphy and G.W. Sears, Appl. Phys. Letters, 3, 55 (1963).

81. W.F. Brown, Jr., J. Appl. Phys., 36, 994 (1965).

82. H.F. Tiersten, J. Math. Phys., 5, 1 (1964); 6, 779 (1965).

83. S. Shtrikman and D. Treves, J. Phys. Radium, 20, 286 (1959).

84. M. Kotrbová and Z. Hauptman, Czech. J. Phys., B15, 64 (1965).

85. D.S. Rodbell, private communication.

86. Z. Frait, private communication.

87. A.J. Melmed and D.O. Hayward, J. Chem. Phys., 31, 545 (1959).

88. G.L. Downs and J.D. Braun, Science, 154, 1444 (1966).

89. B.G. Bagley, Nature, 208, 674 (1965).

GENERAL REFERENCES

I. D.J. Craik and R.S. Tebble, Ferromagnetism and Ferromagnetic Domains, John Wiley and Sons, Inc., New York (1965).

II. S. Chikazumi, Physics of Magnetism, John Wiley and Sons, Inc., New York (1964).

III. M. Prutton, Thin Ferromagnetic Films, Butterworth and Co., Ltd., London (1964).

IV. L.F. Bates, Modern Magnetism, 4th ed., Cambridge Univ. Press, London (1961).

V. S. Middelhoek, Ferromagnetic Domains in Thin Ni-Fe Films, Drukkerij Wed. G. van Soest N.V., Amsterdam (1961).

VI. C. Kittel, Physical Theory of Ferromagnetic Domains, Rev. Mod. Phys., 21, 541 (1949).

VII. R.M. Bozorth, Ferromagnetism, D. Van Nostrand Co., Inc., New York (1951).

Unclassified
Security Classification

**DOCUMENT CONTROL DATA - R&D**

*(Security classification of title, body of abstract and indexing annotation must be entered when the overall report is classified)*

1. ORIGINATING ACTIVITY *(Corporate author)*
General Electric Research and Development Center
Schenectady, New York 12301

2a. REPORT SECURITY CLASSIFICATION
Unclassified

2b. GROUP

3. REPORT TITLE

Ferromagnetic Domain Studies in Highly Perfect Metal Platelets and Whiskers

4. DESCRIPTIVE NOTES *(Type of report and inclusive dates)*
Final Scientific Report

5. AUTHOR(S) *(Last name, first name, initial)*

DeBlois, Ralph W.

| 6. REPORT DATE | 7a. TOTAL NO. OF PAGES | 7b. NO. OF REFS |
|---|---|---|
| March 1967 | 63 | 89 |

| 8a. CONTRACT OR GRANT NO. | 9a. ORIGINATOR'S REPORT NUMBER(S) |
|---|---|
| AF19(628)5804<br>b. PROJECT NO.<br>4600-03, DoD Element No. 62405304<br>c. TASK<br>DoD Subelement No. 674600<br>d. | S-67-1040<br>9b. OTHER REPORT NO(S) *(Any other numbers that may be assigned this report)*<br>AFCRL-67-0107 |

10. AVAILABILITY/LIMITATION NOTICES

DISTRIBUTION OF THIS DOCUMENT IS UNLIMITED

| 11. SUPPLEMENTARY NOTES | 12. SPONSORING MILITARY ACTIVITY |
|---|---|
| -- | Hq. AFCRL, OAR (CRD)<br>United States Air Force<br>L. G. Hanscom Field, Bedford, Mass |

13. ABSTRACT Nearly perfect thin single-crystal platelets and submicron whiskers of nickel and nickel alloy are used to study nearly ideal ferromagnetic domain and domain wall structures and behavior. Applying fields to classically simple domain patterns leads to new observations of surface pinning and to the formation of several new types of double walls. One type is composed of 180° walls of mixed Néel-Bloch structure. Domain observations at the edges and corners of Ni-Co and Ni-Fe platelets with weak negative anisotropy reveal a new "tulip" pattern that makes clear the process of formation of edge echelons and corner chevrons. Precise determinations of saturation fields at platelet corners and ends are made by examining the resulting domain pattern at low field. Nucleation at the corners and edges of previously saturated thin platelets is observable in low positive and negative fields. Further platelet observations include a field induced stripe pattern in Ni-Co platelets with positive anisotropy, domain walls formed by magnetostrictive anisotropy, and

(Abstract continued)

DD FORM 1 JAN 64 1473

Unclassified
Security Classification

Unclassified
Security Classification

| 14. KEY WORDS | LINK A | | LINK B | | LINK C | |
|---|---|---|---|---|---|---|
| | ROLE | WT | ROLE | WT | ROLE | WT |
| Ferromagnetic Domains<br>Domain Walls<br>Ferromagnetic Platelets<br>Whiskers<br>Iron-Nickel<br>Nickel | | | | | | |

## INSTRUCTIONS

1. ORIGINATING ACTIVITY: Enter the name and address of the contractor, subcontractor, grantee, Department of Defense activity or other organization *(corporate author)* issuing the report.

2a. REPORT SECURITY CLASSIFICATION: Enter the overall security classification of the report. Indicate whether "Restricted Data" is included. Marking is to be in accordance with appropriate security regulations.

2b. GROUP: Automatic downgrading is specified in DoD Directive 5200.10 and Armed Forces Industrial Manual. Enter the group number. Also, when applicable, show that optional markings have been used for Group 3 and Group 4 as authorized.

3. REPORT TITLE: Enter the complete report title in all capital letters. Titles in all cases should be unclassified. If a meaningful title cannot be selected without classification, show title classification in all capitals in parenthesis immediately following the title.

4. DESCRIPTIVE NOTES: If appropriate, enter the type of report, e.g., interim, progress, summary, annual, or final. Give the inclusive dates when a specific reporting period is covered.

5. AUTHOR(S): Enter the name(s) of author(s) as shown on or in the report. Enter last name, first name, middle initial. If military, show rank and branch of service. The name of the principal author is an absolute minimum requirement.

6. REPORT DATE: Enter the date of the report as day, month, year, or month, year. If more than one date appears on the report, use date of publication.

7a. TOTAL NUMBER OF PAGES: The total page count should follow normal pagination procedures, i.e., enter the number of pages containing information.

7b. NUMBER OF REFERENCES: Enter the total number of references cited in the report.

8a. CONTRACT OR GRANT NUMBER: If appropriate, enter the applicable number of the contract or grant under which the report was written.

8b, 8c, & 8d. PROJECT NUMBER: Enter the appropriate military department identification, such as project number, subproject number, system numbers, task number, etc.

9a. ORIGINATOR'S REPORT NUMBER(S): Enter the official report number by which the document will be identified and controlled by the originating activity. This number must be unique to this report.

9b. OTHER REPORT NUMBER(S): If the report has been assigned any other report numbers *(either by the originator or by the sponsor)*, also enter this number(s).

10. AVAILABILITY/LIMITATION NOTICES: Enter any limitations on further dissemination of the report, other than those imposed by security classification, using standard statements such as:

(1) "Qualified requesters may obtain copies of this report from DDC."

(2) "Foreign announcement and dissemination of this report by DDC is not authorized."

(3) "U. S. Government agencies may obtain copies of this report directly from DDC. Other qualified DDC users shall request through _____."

(4) "U. S. military agencies may obtain copies of this report directly from DDC. Other qualified users shall request through _____."

(5) "All distribution of this report is controlled. Qualified DDC users shall request through _____."

If the report has been furnished to the Office of Technical Services, Department of Commerce, for sale to the public, indicate this fact and enter the price, if known.

11. SUPPLEMENTARY NOTES: Use for additional explanatory notes.

12. SPONSORING MILITARY ACTIVITY: Enter the name of the departmental project office or laboratory sponsoring *(paying for)* the research and development. Include address.

13. ABSTRACT: Enter an abstract giving a brief and factual summary of the document indicative of the report, even though it may also appear elsewhere in the body of the technical report. If additional space is required, a continuation sheet shall be attached.

It is highly desirable that the abstract of classified reports be unclassified. Each paragraph of the abstract shall end with an indication of the military security classification of the information in the paragraph, represented as *(TS), (S), (C), or (U)*.

There is no limitation on the length of the abstract. However, the suggested length is from 150 to 225 words.

14. KEY WORDS: Key words are technically meaningful terms or short phrases that characterize a report and may be used as index entries for cataloging the report. Key words must be selected so that no security classification is required. Identifiers, such as equipment model designation, trade name, military project code name, geographic location, may be used as key words but will be followed by an indication of technical context. The assignment of links, rules, and weights is optional.

Unclassified
Security Classification

(Abstract continued)

details of spin directions in 180° domain walls with various sequences of Bloch walls, Néel walls, and Bloch lines.

Individual single-domain nickel whiskers as thin as 600 Å have been optically observed, handled, and tested in ferromagnetic nucleation studies. Physical buckling of the whiskers into forms of the elastica permits one to measure both end and infinite-cylinder nucleation fields. Observed fields vs whisker diameter and vs field angle follow curling theory. Thickness comparisons by electron microscopy and by bending yield an effective Young's modulus near $10 \times 10^{11}$ dyn/cm$^2$, about half the handbook value.